Studies of the Boer-Mulders Asymmetry in Kaon Electroproduction with Hydrogen and Deuterium Targets

H. Avakian[†*], A. Bacchetta, V.D. Burkert, L.Elouadrhiri, V. Kubarovsky, S Stepanyan, C. Weiss
Jefferson Lab, Newport News, VA 23606, USA

Z.-E. Meziani[†], B. Sawatzky, A. Lukhanin
Temple University 1900 N. 13th St.Philadelphia, PA 19122, 6082, USA

P.F. Dalpiaz, G. Ciullo, M. Contalbrigo[†], F. Giordano, P. Lenisa, L. Pappalardo
University of Ferrara, Via Paradiso, I-44100, Ferrara, Italy

K. Joo[†], P. Schweitzer, M. Ungaro
University of Connecticut, Storrs, CT 06269, USA

D. Ireland, R. Kaiser, K. Livingston, D. MacGregor, G. Rosner, B. Seitz[†]
Univ. of Glasgow, Glasgow G12 8QQ, UK

E. Cisbani, F. Cusanno, F. Garibaldi, S. Frullani
INFN Roma I and Istituto Superiore di Sanita', I-00161 Rome, Italy

P. Rossi, E. De Sanctis, L. Hovsepyan, M. Mirazita, and S. Anefalos Pereira
INFN, Laboratori Nazionali di Frascati , Via E. Fermi, I-00044 Frascati, Italy

M. Battaglieri, R. De Vita, V. Drozdov, M. Osipenko, M. Ripani, M. Taiuti
Dipartamento di Fisica and INFN, Sezione di Genova, Via Dodecaneso, 33 I-16146 Genova, Italy

V. Bellini, A. Giusa, F. Mammoliti, C. Randieri, G. Russo, M.L. Sperduto, C.M. Sutera
INFN - Sezione di Catania and Universita' di Catania, I-95123 Catania, Italy

K. Hafidi, J. Arrington, R. Dupré, D. F. Geesaman, R. J. Holt
D. H. Potterveld, P. E. Reimer, P. Solvignon
Argonne National Lab, Argonne, IL 60439, USA

M. Aghasyan, S.E. Kuhn Old Dominion University, Norfolk, VA 23529, USA

K. Griffioen, Bo Zhao, College of William & Mary, VA 23187, USA

A. D'Angelo, C. Schaerf, V. Vegna
INFN Sezione di Roma Tor Vergata, Via della Ricerca Scientifica 1- I00133, Rome, Italy

R. De Leo, L. Lagamba, S. Marrone, G. Simonetti, E. Nappi, I. Vilardi
INFN Sezione di Bari and University of Bari, 70126 Bari, Italy

G.M. Urciuoli, INFN Roma I, I-00161 Rome, Italy

N. Kalantarians, D. Crabb, L.C. Smith, UVA, Charlottesville, VA 22904,USA

R. Avagyan, A. Avetisyan, R. Dallakyan, S. Taroyan
Yerevan Physics Institute, Alikhanian Br. 2, Yerevan, Armenia

F. Benmokhtar, Carnegie Mellon University, 5000 Forbes Avenue, Pittburgh, PA 15213, USA

M. Anselmino, A. Kotzinian, B. Parsamyan, A. Prokudin
Università di Torino and INFN, Sezione di Torino, Via P. Giuria 1, I-10125 Torino
M. Burkardt New Mexico State University, PO Box 30001, Las Cruces, NM 88003, USA
B. Pasquini, Universita degli Studi di Pavia, Pavia, Italy
Zhun Lu, Universidat Tecnica Federico Santa Maria, Casilla 110-V, Valparaiso, Chile
Bing Zhang, Bo-Qiang Ma, Peking University, Beijing 100871,China
L. Gamberg, Penn State Berks, Reading, PA 19610, USA
G.R. Goldstein, Tufts University, Medford, MA 02155, USA

A CLAS collaboration proposal

† Co-spokesperson * Contact: Harut Avakian, JLab, Newport News VA 23606. Email: avakian@jlab.org

Collaborators' commitment to the 12 GeV upgrade of Jefferson Lab

- ### Italian JLAB12 collaboration

  The Italian JLAB12 collaboration (INFN Bari, INFN Catania, Laboratori Nazionali di Frascati, INFN Genova, INFN Roma I and Istituto Superiore di Sanita', INFN Roma Tor Vergata) is actively involved in this proposal. Among CLAS12 equipment, the group plans to contribute to the design, prototyping, construction and testing of the CLAS12 RICH detector and central calorimeter. Seven staff members and three post-docs will spend their time as needed on this project. Funding for the group is from the Italian research agency Istituto Nazionale di Fisica Nucleare (INFN). Additional funding are planned to be sought in the European Community.

- ### Temple University

  Temple University's group has one faculty member (Z.-E. Meziani), a post-doc(B. Sawatzky), a research associate (A. Lukhanin) and several graduate students. The major source of funding for the group is DOE, however, the research associate is only paid half by DOE the other half of his salary is provided by the University. The intended contribution is 1 FTE-year for the Cherenkov counter installation and commissioning as well as the analysis of the experiment.

- ### Glasgow University

  The Glasgow University group is actively involved in this proposal, as well as in another proposal using CLAS12; one proposal for Hall A and the GlueX proposal.

  The Glasgow group plans to contribute to the design, prototyping, construction, and testing of the following CLAS12 baseline equipment: silicon vertex tracker electronic readout system, data acquisition, GRID computing, photon beamline. Beyond the baseline equipment, the group is also interested in building a RICH detector for kaon identification in CLAS12.

  Seven faculty members and research staff and four technicians/engineers are likely to work at least part time on this project in the next few years. Funding for the group is from the UK Science and Technology facilities Council (STFC). Additional sources of funding will be sought as appropriate.

- ### University of Connecticut

  The University of Connecticut (UConn) group is actively involved in this proposal using CLAS12 baseline equipment. Among the CLAS12 baseline equipment projects, the UConn group has taken responsibility for (1) the development of the CLAS12 detector simulation program based on Geant4-software-toolkit, and (2) the design, prototyping,

construction and testing of the high threshold Cerenkov counter (HTCC). One faculty member (K. Joo), one research associate (M. Ungaro), six graduate students are already or will be working at least part time on the CLAS12 project for the next few years. The group is currently funded by the U.S Department of Energy (DOE) and the University of Connecticut Research Foundation (UCRF). Additional sources of funding will be sought as appropriate

Abstract

We are proposing a comprehensive program to study transverse momentum dependence of valence quark transverse spin distributions through measurements of spin-azimuthal asymmetries in semi-inclusive electroproduction of kaons using the upgraded JLab 11 GeV polarized electron beam and the CLAS12 detector with unpolarized proton and deuteron targets. The main objective is the study of correlations of the transverse spin of quarks with their transverse momentum, leading to observable spin and azimuthal asymmetries. The measurement of the $\cos 2\phi$ azimuthal moments of the semi-inclusive production of hadrons in DIS with unpolarized targets, in particular, will provide direct information on spin-orbit correlations by measuring the leading twist transverse momentum dependent (TMD) parton distributions related to the interference between states with different orbital momenta. Measurements with kaons are complementary to measurements with pions and will provide additional information on the Collins fragmentation mechanism. The x, z, P_T and Q^2 dependences of the $\cos 2\phi$ moment will be studied to probe the underlying T-odd distribution and fragmentation functions. The experiment will use the upgraded CLAS12 detector, 11 GeV highly polarized electron beam, unpolarized hydrogen and deuteron, targets. Kaon identification in the complete kinematic range will be done by the proposed CLAS12-RICH proximity-focusing detector. The large acceptance of CLAS12 would allow simultaneous detection of the scattered electrons and leading hadrons from the hadronization of the struck quark, providing information on its flavor and transverse momentum. We request 56 days of running on unpolarized hydrogen and deuterium. This measurement will simultaneously run with an already approved electroproduction experiment.

Contents

1 Introduction

Semi-inclusive deep inelastic scattering (SIDIS) has been used extensively in recent years as an important testing ground for QCD. Studies so far have concentrated on better determination of parton distribution functions, distinguishing between the quark and antiquark contributions, and understanding the fragmentation of quarks into hadrons. The use of polarization in leptoproduction provides an essential new dimension for testing QCD. The spin structure of the nucleon has been of particular interest since the EMC [1] measurements implied that the helicity of the constituent quarks account for only a fraction of the nucleon spin. Possible interpretations of the small fraction of the spin carried by quark helicities include the contribution of the orbital momentum of quarks and gluons and significant polarization of either the strange sea (negatively polarized) or gluons (positively polarized).

Azimuthal distributions of final state particles in semi-inclusive deep inelastic scattering are sensitive to the orbital motion of quarks and play an important role in the study of transverse momentum distributions of quarks in the nucleon. Correlations of spin and transverse momentum of quarks are by now universally recognized as essential ingredients of the structure of hadrons. They are described by a number of Transverse Momentum dependent Distribution functions (TMDs) [2, 3] which give rise to various observables in hard hadronic processes [4].

Large Single Spin Asymmetries (SSAs), have been among the most difficult phenomena to understand from first principles in QCD and can also be related to TMDs. Two fundamental mechanisms have been identified leading to SSAs in hard processes; the Sivers mechanism [5, 6, 7, 8, 9], which generates an asymmetry in the distribution of quarks due to orbital motion of partons, and the Collins mechanism [8, 2], which generates an asymmetry during the hadronization of quarks.

Significant progress has been made recently in understanding the role of partonic initial and final state interactions [7, 8, 9]. The interaction between the active parton in the hadron and the spectators was included in gauge-invariant TMD distributions [7, 8, 9, 10, 11]. Furthermore, QCD factorization for semi-inclusive deep inelastic scattering at low transverse momentum in the current-fragmentation region has been established in Refs. [12, 13]. This new framework provides a rigorous basis to study the TMD parton distributions from SIDIS data using different spin-dependent and independent observables. TMD distributions (see Table 1) describe transitions of a nucleon with one polarization in the initial state to a quark with another polarization in the final state.

The diagonal elements of the table are the momentum, longitudinal and transverse spin distributions of partons, and represent well-known parton distribution functions related to the square of the leading-twist, light-cone wave functions. Off-diagonal elements require non-zero orbital angular momentum and are related to the overlap of light-cone wave functions with $\Delta L \neq 0$ [14]. The parton distributions $f_{1T}^{\perp}$ and $h_1^{\perp}$ represent the imaginary parts of the corresponding interference terms, while the functions g_{1T} and $h_{1L}^{\perp}$ represent their real parts. The TMDs $f_{1T}^{\perp}$ (chiral-even) and $h_1^{\perp}$ (chiral-odd) are known as the Sivers and Boer-Mulders functions, respectively [5, 6, 15, 8, 9, 10]. They describe unpolarized quarks in the transversely polarized nucleon and transversely polarized quarks in the unpolarized nucleon respectively. They vanish at tree-level in a T-reversal invariant model (T-odd) and can only be non-zero when initial or final state interactions cause an interference between

N \ q	U	L	T
U	$\mathbf{f_1}$		$h_1^\perp$
L		$\mathbf{g_1}$	$h_{1L}^\perp$
T	$f_{1T}^\perp$	g_{1T}	$\mathbf{h_1}$ $h_{1T}^\perp$

Table 1: Leading-twist transverse momentum-dependent distribution functions. U, L, and T stand for transitions of unpolarized, longitudinally polarized, and transversely polarized nucleons (rows) to corresponding quarks (columns), respectively.

different helicity states. These functions parametrize the correlation between the transverse momentum of quarks and the spin of a transversely polarized target or the transverse spin of the quark, respectively. They require both orbital angular momentum, as well as non-trivial phases from the final state interaction that survive in the Bjorken limit. The T-even counterpart of the Boer-Mulders function, $h_{1L}^\perp$, first introduced by Ralston and Soper [16], describes the correlations of the transverse spin of quarks in the longitudinally polarized nucleon and their transverse momentum.

Parton distribution and fragmentation functions in DIS, Drell-Yan, and electron-positron annihilation have different gauge links, which raised a question of the universality of those functions [13, 11, 17]. It has been found that all six T-even TMD parton distributions are the same in SIDIS and Drell-Yan. The violation of universality for T-odd distributions appeared to be just a sign reversal from DIS to Drell-Yan, an exciting prediction that has to be confirmed by future experiments. Universality of TMDs in processes with hadrons in both initial and final states is violated, at least in its standard form [18, 17, 19], with far-reaching consequences in hadron collider physics.

Similar correlations arise in the hadronization process. One particular case is the Collins T-odd fragmentation function $H_1^\perp$ [20], describing fragmentation of transversely polarized quarks into unpolarized hadrons. The Collins function is one of the most fundamental quantities accessible in hard fragmentation processes. It is of essential importance for spin physics because it works as an analyzer of the spin of the quark, but it is also interesting on its own because it allows the exploration of spin and orbital degrees of freedom of the QCD vacuum. It is universal [21, 13, 22], once measured in e^+e^-, it can be used in SIDIS and pp collisions and vice versa. For kaons in particular, the u to kaons Collins fragmentation function allows for exploring the structure of the strange vacuum, while the s to kaons Collins function allows for study the spin structure of the strangeness in the nucleon.

In recent years, measurements of azimuthal moments of hadronic cross sections in hard processes have emerged as a powerful tool to probe nucleon structure through transverse single spin asymmetries. Many experiments worldwide are currently trying to pin down various TMD effects through semi-inclusive deep-inelastic scattering (in experiments such as HERMES at DESY [23, 24, 25, 26], COMPASS at CERN [27], CLAS and Hall-A at Jefferson Lab [28, 29]), polarized proton-proton collisions (PHENIX, STAR and BRAHMS at RHIC) [30, 31, 32], and electron-positron annihilation (Belle at KEK) [33]. In contrast to inclusive deep inelastic lepton-nucleon scattering where transverse momentum is integrated out, these processes are sensitive to transverse momentum scales on the order of the intrinsic quark

momentum $P_T \sim k_\perp$.

The JLab 12-GeV upgrade will provide the unique combination of wide kinematic coverage, high beam intensity (luminosity), high energy, high polarization, and advanced detection capabilities necessary to study the transverse momentum and spin correlations in semi-inclusive processes both in the target and current fragmentation regions for a variety of hadron species. In this proposal we focus on observables related to kaon production in DIS, accessible with unpolarized targets and new information on the structure of nucleon they can provide. Measurements of spin-orbital structure of hadrons with unpolarized hydrogen and deuterium targets will use the beam time of an already approved electroproduction experiment to study the Neutron Magnetic Form-Factor at High Q^2 [34].

1.1 Spin and Azimuthal Asymmetries in SIDIS

The SIDIS cross section at leading twist has eight contributions related to different combinations of the polarization state of the incoming lepton and the target nucleon [35, 2, 12, 3]. The lepton-hadron cross section can then be parametrized as [3]

$$\begin{aligned}
\frac{d\sigma}{dx\,dy\,dz\,d\phi_S\,d\phi_h\,dP_{h\perp}^2} &= \frac{\alpha^2}{xQ^2}\,\frac{y}{2\,(1-\varepsilon)} \\
&\times \Big\{ F_{UU,T} + \varepsilon\cos(2\phi_h)\,F_{UU}^{\cos 2\phi_h} + S_L\,\varepsilon\sin(2\phi_h)\,F_{UL}^{\sin 2\phi_h} \\
&\quad + S_L\lambda_e\sqrt{1-\varepsilon^2}\,F_{LL} + |\boldsymbol{S}_T|\,\Big[\sin(\phi_h-\phi_S)\,F_{UT,T}^{\sin(\phi_h-\phi_S)} \\
&\qquad + \varepsilon\,\sin(\phi_h+\phi_S)\,F_{UT}^{\sin(\phi_h+\phi_S)} + \varepsilon\,\sin(3\phi_h-\phi_S)\,F_{UT}^{\sin(3\phi_h-\phi_S)}\Big] \\
&\quad + |\boldsymbol{S}_T|\,\lambda_e\Big[\sqrt{1-\varepsilon^2}\,\cos(\phi_h-\phi_S)\,F_{LT}^{\cos(\phi_h-\phi_S)}\Big]\Big\}\,,
\end{aligned} \tag{1}$$

where α is the fine structure constant and ε the ratio of longitudinal and transverse photon flux,

$$\varepsilon = \frac{1-y}{1-y+y^2/2}\,. \tag{2}$$

The kinematic variables x and y are defined as: $x = Q^2/2(P_1q)$, and $y = (P_1q)/(P_1k_1)$, respectively. The variable $q = k_1 - k_2$ is the momentum of the virtual photon, $Q^2 = -q^2$, ϕ_h is the azimuthal angle between the scattering plane formed by the initial and final momenta of the electron and the production plane formed by the transverse momentum of the observed hadron and the virtual photon (see Fig. 1), and ϕ_S is the azimuthal angle of the transverse spin in the scattering plane. The subscripts in F_{UL}, F_{LL},etc., specify the beam (first index) and target(second index) polarizations, longitudinal (L), transverse (T), and unpolarized (U).

Structure functions factorize into TMD parton distributions, fragmentation functions, and hard parts [12, 3]

$$\begin{aligned}
\sigma_{UU} \propto F_{UU} \propto \quad & f_1\left(x, k_\perp\right) D_1\left(z_h, p_\perp\right) H_{UU}\left(Q^2\right) \\
\sigma_{LL} \propto F_{LL} \propto \quad & g_{1L}\left(x, k_\perp\right) D_1\left(z_h, p_\perp\right) H_{LL}\left(Q^2\right) \\
\sigma_{UL} \propto F_{UL} \propto \quad & h_{1L}^\perp\left(x, k_\perp\right) H_1^\perp\left(z_h, p_\perp\right) H_{UL}\left(Q^2\right),
\end{aligned} \tag{3}$$

where $z = (P_1 P_h)/(P_1 q)$, $k_\perp$ and $p_\perp$ are quark transverse momenta before and after scattering, respectively and P_1 and P_h are the four momenta of the initial nucleon and the observed final-state hadron, respectively.

The unpolarized D_1 and polarized $H_1^\perp$ fragmentation functions depend in general on the transverse momentum of the fragmenting quark.

S_L and S_T are longitudinal and transverse components of the target polarization with respect to the direction of the virtual photon. The different hard factors (H_{UU}, H_{LL},etc.), which are calculable in pQCD, in the SIDIS cross section are similar at one-loop order [12] and may cancel to a large extent in asymmetry observables.

In the case of the polarized beam and unpolarized or longitudinally polarized target the cross section in the leading order has only two contributions that depend on the azimuthal angle of the final state hadron, appearing as $\cos 2\phi$ and $\sin 2\phi$ modulations, involving four leading twist TMD distribution functions [2, 36, 35].

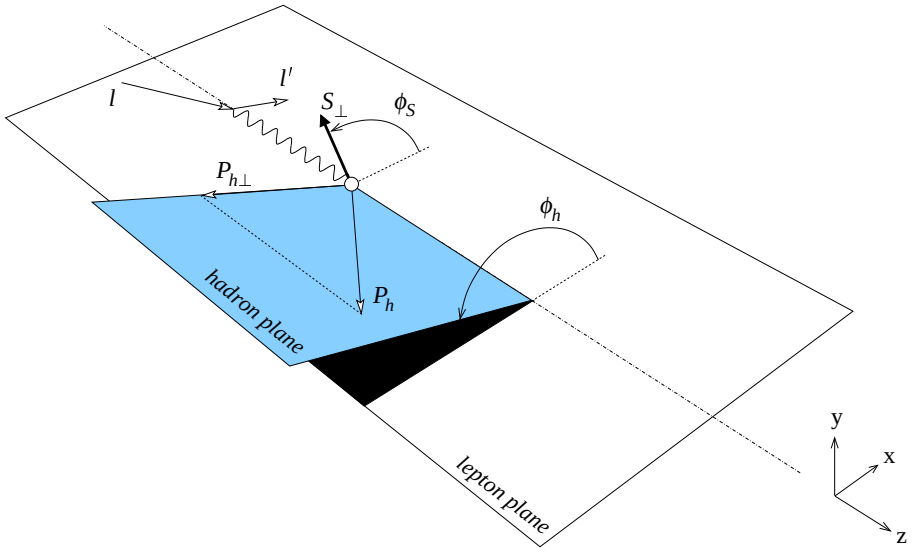

Figure 1: SIDIS kinematics. For a longitudinally polarized target, ϕ_S=0 or 180^o for negative and positive helicities of the proton, respectively.

During the last few years, first results on transverse SSAs have become available [25, 27]. Pioneering measurements by the HERMES Collaboration for the first time directly indicated significant azimuthal moments generated both by Collins ($F_{UT}^{\sin(\phi+\phi_S)}$) and Sivers ($F_{UT}^{\sin(\phi-\phi_S)}$) effects. Significant differences were observed between charged pion and kaon, both for Sivers and Collins effects (see Fig.2). Currently no satisfactory explanation exists for these observed differences.

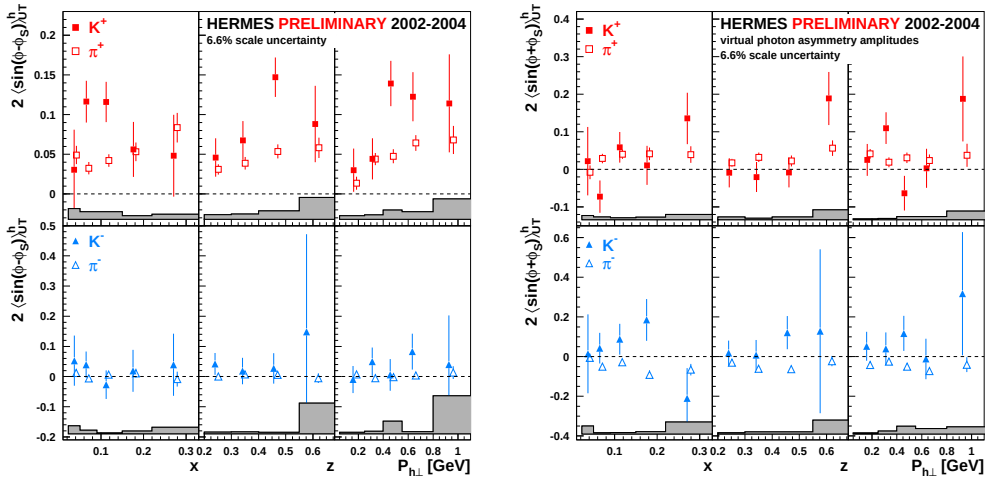

Figure 2: First measurements of Collins (right) and Sivers(left) asymmetries for pions and kaons.

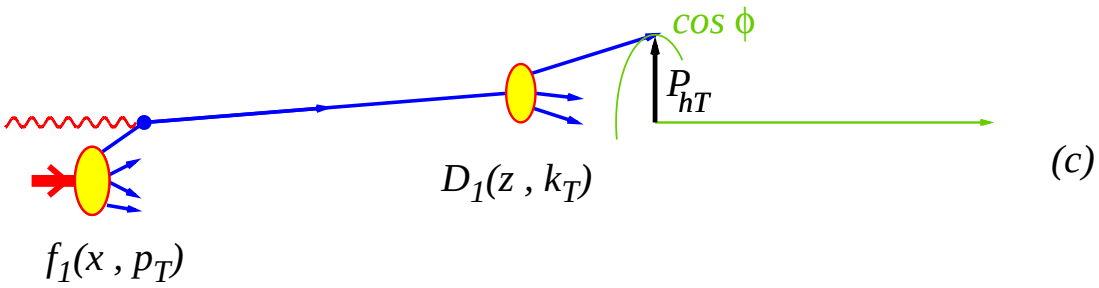

Figure 3: Cahn effect from intrinsic transverse parton momenta [37]

1.1.1 Azimuthal Asymmetries in unpolarized SIDIS

Spin-orbit correlations are accessible in SIDIS with unpolarized target in measurements of azimuthal distributions of hadrons as well as cross section measurements as a function of their transverse momentum.

In the collinear limit of QCD, integrating over the transverse momentum, integrated ($f_1^a(x) = \int \mathrm{d}^2\mathbf{p}_T f_1(x, \mathbf{p}_T)$) and FFs ($D_1^a(z) = \int \mathrm{d}^2\mathbf{k}_T D_1(z, \mathbf{k}_T)$) remain, so the azimuthal dependences due to correlations of transverse momentum of partons and their spin vanish.

Within the leading order (zero-th order in α_s) parton model with twist-two distribution and fragmentation functions (FFs), the simplest azimuthal asymmetry, a $\cos\phi_h$ dependence, arises in unpolarized SIDIS (the so-called Cahn effect [37]). It accounts for the partons intrinsic transverse momenta in the target (p_T) and the fact that produced hadrons (Fig.3) may acquire transverse momenta from the fragmentation process (k_T), so that final hadron transverse momentum P_T is defined as their sum ($P_T = zp_T + k_T$). Within the same approach, kinematical corrections proportional to $(k_\perp/Q)^2$ lead to additional contributions in the $\cos 2\phi_h$ moment.

For a unpolarized target the only azimuthal asymmetry arising in leading order is the

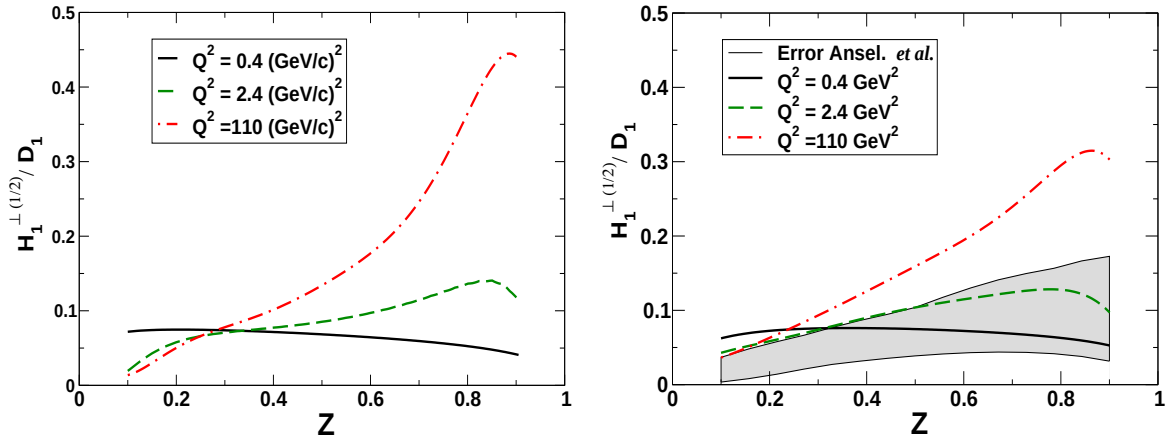

Figure 4: $H_1^{\perp(1/2)}/D_1$ for $u \to K^+$ (left) and π^+ (right) in the model of Bacchetta et al.[48], at the model scale (solid line) and at two other scales (dashed and dot-dashed lines) under the assumption that the Collins function does not evolve with the scale.

$\cos 2\phi$ moment,

$$\sigma_{UU}^{\cos 2\phi} \propto 2(1-y)\cos 2\phi \sum_{q,\bar{q}} e_q^2 x h_1^{\perp q}(x) \otimes H_1^{\perp q}(z). \tag{4}$$

The Boer-Mulders distribution function, $h_1^\perp$, giving rise to the asymmetry, is related to the imaginary part of the interference of wave functions for different orbital momentum states, and describes transversely polarized quarks in the unpolarized nucleon. The physics of σ_{UU}, which involves the Collins fragmentation function $H_1^\perp$ and the Boer-Mulders distribution function $h_1^\perp$, was first discussed by Boer and Mulders in 1997 [36]. The same distribution function is accessible in the unpolarized Drell-Yan, where it gives rise to the $\cos 2\phi$ azimuthal moment in the cross section [38], which is the target of the planned E906 experiment at Fermilab [39]. The behavior of the Boer-Mulders distribution function was recently studied in large-x [40], large N_c [41], and large P_T [42] limits of QCD. There are Boer-Mulders asymmetry predictions for various models [43, 44, 45, 46], for all DIS and DY experiments.

The extraction of the Boer-Mulders transverse momentum dependent distributions is complicated by the presence of an essentially unknown Collins function. Recently a significant asymmetry was measured by Belle [33] in e^+e^- annihilation to pions, indicating that the Collins function is indeed large. Based on leading order, a procedure has been developed recently [47] to extract the transversity distribution, combining e^+e^- and semi-inclusive DIS data [25].

So far no experimental information is available about the Collins fragmentation function for kaons. Recent direct calculations of kaon Collins function [48] indicated that it may be comparable with pion Collins function (see Fig.4). HERMES measurements of the Collins asymmetry for pions and kaons, though, with large uncertainties, indicate that the differences may be significant.

Pions and kaons are both Goldstone bosons of chiral symmetry breaking. In the chiral

limit one has

$$\lim_{m_K\to 0}\frac{H_1^{\perp(1/2)a/K}}{D_1^{a/K}}=\lim_{m_\pi\to 0}\frac{H_1^{\perp(1/2)a/\pi}}{D_1^{a/\pi}}\ , \tag{5}$$

where $H_1^{\perp(1/2)}$ means integration over the transverse momentum weighted with k_T. Predictions for kaon Collins asymmetries assume the following relations to hold approximately

$$\frac{H_1^{\perp(1/2)\bar{s}/K^+}}{D_1^{\bar{s}/K^+}}\approx\frac{H_1^{\perp(1/2)u/K^+}}{D_1^{u/K^+}}\approx\frac{H_1^{\perp(1/2)u/\pi^+}}{D_1^{u/\pi^+}}\,,$$

$$\frac{H_1^{\perp(1/2)\mathrm{unf}/K^+}}{D_1^{\mathrm{unf}/K^+}}\approx\frac{H_1^{\perp(1/2)\mathrm{unf}/\pi^+}}{D_1^{\mathrm{unf}/\pi^+}}\ , \tag{6}$$

where it is understood that the fragmentation of d- and $\bar{u}$-flavour into K^+ is unfavoured.

Simultaneous measurements of the Boer-Mulders asymmetry for pions and kaons will provide an independent measurement of ratios of Collins functions of pions and kaons, providing complementary measurements to e^+e^- annihilation.

The $\cos 2\phi$ moments ($\langle\sigma_{UU}^{\cos 2\phi}\rangle\equiv\sigma_{BM}$) in the unpolarized cross section, coming from the polarized fragmentation for different hadrons in the leading order for hydrogen (p) and neutron (n) targets are given by:

$$\sigma_{BM}^{\pi+}(p)=4h_1^{\perp u}H_1^{\perp(1/2)fav}+h_1^{\perp d}H_1^{\perp(1/2)unfav} \tag{7}$$
$$\sigma_{BM}^{\pi-}(p)=4h_1^{\perp u}H_1^{\perp(1/2)unfav}+h_1^{\perp d}H_1^{\perp(1/2)fav} \tag{8}$$
$$\sigma_{BM}^{\pi0}(p)=4(h_1^{\perp u}+h_1^{\perp d})(H_1^{\perp(1/2)unfav}+H_1^{\perp(1/2)fav}) \tag{9}$$
$$\sigma_{BM}^{K+}(p)=4h_1^{\perp u}H_1^{\perp(1/2)u/K^+}+h_1^{\perp d}H_1^{\perp(1/2)d/K^+}+h_1^{\perp\bar{s}}H_1^{\perp(1/2)\bar{s}/K^+} \tag{10}$$
$$\sigma_{BM}^{K-}(p)=4h_1^{\perp u}H_1^{\perp(1/2)u/K^-}+h_1^{\perp d}H_1^{\perp(1/2)d/K^-}+h_1^{\perp s}H_1^{\perp(1/2)s/K^-}+4h_1^{\perp\bar{u}}H_1^{\perp(1/2)\bar{u}/K^-} \tag{11}$$
$$\sigma_{BM}^{\pi+}(n)=4h_1^{\perp d}H_1^{\perp(1/2)fav}+h_1^{\perp u}H_1^{\perp(1/2)unfav} \tag{12}$$
$$\sigma_{BM}^{\pi-}(n)=4h_1^{\perp d}H_1^{\perp(1/2)unfav}+h_1^{\perp u}H_1^{\perp(1/2)fav} \tag{13}$$
$$\sigma_{BM}^{\pi0}(n)=(4h_1^{\perp d}+h_1^{\perp u})(H_1^{\perp(1/2)unfav}+H_1^{\perp(1/2)fav}) \tag{14}$$
$$\sigma_{BM}^{K+}(n)=4h_1^{\perp d}H_1^{\perp(1/2)u/K^+}+h_1^{\perp u}H_1^{\perp(1/2)d/K^+}+h_1^{\perp\bar{s}}H_1^{\perp(1/2)\bar{s}/K^+} \tag{15}$$
$$\sigma_{BM}^{K-}(n)=4h_1^{\perp d}H_1^{\perp(1/2)u/K^-}+h_1^{\perp u}H_1^{\perp(1/2)d/K^-}+h_1^{\perp s}H_1^{\perp(1/2)s/K^-}+h_1^{\perp\bar{u}}H_1^{\perp(1/2)\bar{u}/K^-} \tag{16}$$

Assuming that the transverse spin of the sea quarks in unpolarized nucleon is negligible ($h_1^{\perp\bar{q}}=0$) and ignoring the non-valence quark contributions in K^+ production and unfavored fragmentation, the contribution to the $\cos 2\phi$ moment arising from fragmentation becomes:

$$A_{UU}^{K^+}\propto\frac{4h_1^{\perp(1)u}(x)}{4u(x)+\bar{s}(x)}\frac{H_1^{\perp u\to K^+}(z,P_\perp)}{D_1^{u\to K^+}(z,P_\perp)}, \tag{17}$$

where $h_1^{\perp(1)}$ means integration over the transverse momentum weighted with k_T^2. Similar formulas apply to the neutron target replacing u and d and also for K^-. For them, however,

the contribution from unfavored fragmentation will be significant and should be accounted in the extraction.

Assuming isospin and charge-conjugation relations, there are in principle seven independent Collins fragmentation functions, but based on the observation that the pion favored Collins function is roughly equal and opposite to the unfavored one, the number of independent Collins functions could be reduced to three.

The asymmetries built from the difference between π^+ and π^- and of the K^+ and K^- observables give (see Appendix-I)

$$A^{p/(\pi^+-\pi^-)}(x,y,z) = 2\frac{B(y)}{A(y)}\frac{\left(4\,h^{u_v} - h^{d_v}\right)H_1^{\perp(1)\mathrm{f}}}{\left(4\,f_1^{u_v} - f_1^{d_v}\right)\left(D_1^{\mathrm{f}} - D_1^{\mathrm{d}}\right)}, \tag{18}$$

$$A^{n/(\pi^+-\pi^-)}(x,y,z) = 2\frac{B(y)}{A(y)}\frac{\left(4\,h^{d_v} - h^{u_v}\right)H_1^{\perp(1)\mathrm{f}}}{\left(4\,f_1^{d_v} - f_1^{u_v}\right)\left(D_1^{\mathrm{f}} - D_1^{\mathrm{d}}\right)}, \tag{19}$$

$$A^{p/(K^+-K^-)}(x,y,z) = 2\frac{B(y)}{A(y)}\frac{4\,h^{u_v}\,H_1^{\perp(1)\mathrm{fd}} - h^{s_v}\,H_1^{\perp(1)\mathrm{f}'}}{4\,f_1^{u_v}\left(D_1^{\mathrm{fd}} - D_1^{\mathrm{dd}}\right) + f_1^{s_v}\left(D_1^{\mathrm{d}'} - D_1^{\mathrm{f}'}\right)}, \tag{20}$$

$$A^{n/(K^+-K^-)}(x,y,z) = 2\frac{B(y)}{A(y)}\frac{4\,h^{d_v}\,H_1^{\perp(1)\mathrm{fd}} - h^{s_v}\,H_1^{\perp(1)\mathrm{f}'}}{4\,f_1^{d_v}\left(D_1^{\mathrm{fd}} - D_1^{\mathrm{dd}}\right) + f_1^{s_v}\left(D_1^{\mathrm{d}'} - D_1^{\mathrm{f}'}\right)}. \tag{21}$$

The s_v superscript refers to the difference between s and $\bar{s}$. $A(y)$ and $B(y)$ are kinematic factors [3].

Neglecting the s_v contributions and the "unfavored " D_1^{dd} fragmentation function (FF), the "kaon differences" asymmetries simplify to

$$A^{p/(K^+-K^-)}(x,y,z) = 2\frac{B(y)}{A(y)}\frac{h^{u_v}}{f_1^{u_v}}\frac{H_1^{\perp(1)\mathrm{fd}}}{D_1^{\mathrm{fd}}}, \tag{22}$$

$$A^{n/(K^+-K^-)}(x,y,z) = 2\frac{B(y)}{A(y)}\frac{h^{d_v}}{f_1^{d_v}}\frac{H_1^{\perp(1)\mathrm{fd}}}{D_1^{\mathrm{fd}}}. \tag{23}$$

where the index "fd" indicates favored kaon FFs. The z dependence of the above asymmetries is predicted to follow the curve in Figure 4.

In the approximation of strangeness contribution being negligible in the valence region one can write:

$$\frac{H_1^{u/K+} - H_1^{u/K-}}{H_1^{u/\pi+} - H_1^{u/\pi-}} = \frac{15}{4}\frac{F_p^{K+} - F_p^{K-}}{3(F_p^{\pi+} - F_p^{\pi-}) + (F_d^{\pi+} - F_d^{\pi-})}, \tag{24}$$

where F_{target}^{hadron} can be any one of four Collins asymmetries related to $H_1^{\perp}$, like $\langle\cos 2\phi\rangle_{UU}$, $\langle\sin 2\phi\rangle_{UL}$, $\langle\sin(\phi+\phi_S)\rangle_{UT}$ or $\langle\sin(3\phi-\phi_S)\rangle_{UT}$.

There are indications from Collins asymmetry measurements [25] that $H_1^{u/\pi+} - H_1^{u/\pi-}$ is large, and that will allow precision measurement of kaon Collins function, under the assumptions discussed above. That measurement will also provide a check of chiral limit prediction, where that ratio is expected to be at unity. More ratios could be constructed

from other observable moments with pions and kaons on proton and deuteron targets. With a given Collins function, one can study all involved TMD distributions.

Measurements of transverse momenta of final state hadrons in SIDIS with unpolarized targets will thus provide information on the polarized Collins fragmentation of kaons complementary to transverse target and future measurements in e^+e^- by BELLE.

Measurement of the fraction coming from the Collins fragmentation of transversely polarized quarks in the unpolarized nucleon will require separation of other contributions, and in particular those due to the Cahn effect. Although, preliminary results from HERMES indicate that the Cahn contribution is not dominant in $\cos 2\phi$ as was expected before [49]. In order to extract the contribution related to the Collins fragmentation one needs a reliable calculation of the kinematical corrections. Perturbative QCD contributions (at order α_s and possibly α_s^2) to the kinematical $\cos\phi_h$ and $\cos 2\phi_h$ asymmetries also have to be evaluated. Such a study shows that the parton model with TMD DFs and FFs dominates at P_T values below 1 (GeV/c) [49].

We propose a measurement of azimuthal moments of the single kaon cross section in SIDIS using the CLAS12 detector in Hall B at Jefferson Lab, a 6.6-11.0 GeV longitudinally polarized electron beam and unpolarized hydrogen and deuterium targets. The focus of our proposal is to study the $\cos 2\phi$ asymmetry, related to the correlation of intrinsic transverse momentum of quarks and their transverse spin. Competing mechanisms are also related to the transverse motion of quarks and are also relevant in the CLAS12 kinematic regime ($\langle Q^2\rangle \sim 2$ GeV^2).

The overall statistics of kaons is almost an order of magnitude less than for pions with most of the relevant sources of systematic errors being the same, so the main focus will be the new information we can access with kaon SIDIS measurements and in particular studies of the Collins fragmentation of kaons.

1.2 Transverse momentum dependence of partonic distributions

Assuming the Gaussian ansatz for distribution and fragmentation functions ($D_1(z,\mathbf{K}_T) = D_1^a(z)\,\exp(-\mathbf{K}_T^2/\langle K_{D_1}^2\rangle)/\pi\langle K_{D_1}^2\rangle$ and $f_1^a(x,\mathbf{p}_T) = f_1^a(x)\,\exp(-\mathbf{p}_T^2/\langle \mathbf{p}_T^2\rangle)/\pi\langle \mathbf{p}_T^2\rangle$) in the approximation of flavor and x or z-independent widths, a good quantitative description of data was obtained [49] for

$$\langle p_T^2\rangle = 0.25\,\mathrm{GeV}^2\,, \quad \langle K_{D_1}^2\rangle = 0.20\,\mathrm{GeV}^2\,. \tag{25}$$

Assuming the Gaussian model, the average $P_{h\perp}$ of hadrons produced in SIDIS is given by

$$\langle P_{h\perp}(z)\rangle \;=\; \frac{\sqrt{\pi}}{2}\,\sqrt{z^2\langle p_T^2\rangle + \langle K_{D_1}^2\rangle}\,. \tag{26}$$

A satisfactory description with HERMES data [50] on deuteron was obtained [51] with

$$\langle p_T^2\rangle = 0.33\,\mathrm{GeV}^2\,, \quad \langle K_{D_1}^2\rangle = 0.16\,\mathrm{GeV}^2\,. \tag{27}$$

The width for different partonic distributions can be different. Values for different T-even partonic distributions, computed [52] in the constituent quark model [53] are listed in

TMD	$\langle p_T \rangle$ in GeV	$\langle p_T^2 \rangle$ in GeV^2	$\frac{4\langle p_T \rangle^2}{\pi \langle p_T^2 \rangle}$
f_1	0.239	0.080	0.909
g_1	0.206	0.059	0.916
h_1	0.210	0.063	0.891
$g_{1T}^{\perp}$	0.373	0.176	1.007
$h_{1L}^{\perp}$	0.373	0.176	1.007
$h_{1T}^{\perp}$	0.190	0.050	0.919

Table 2: The mean transverse momenta and the mean square transverse momenta of T-even TMDs, from the constituent quark model [53]. If the transverse momenta in the TMDs were Gaussian, then the result for the ratio in the last row would be unity (see text).
2cm

TMD	$\frac{\langle p_T^2 \rangle}{\langle p_{Tf_1}^2 \rangle}$
f_1	1.00
g_1	0.74
h_1	0.79
$g_{1T}^{\perp}$	2.20
$h_{1L}^{\perp}$	2.20
$h_{1T}^{\perp}$	0.63

Table 3: Mean square transverse momenta of T-even TMDs, from the constituent quark model [53] in units of the mean square transverse momenta of f_1, denoted as $\langle p_{Tf_1}^2 \rangle$. These numbers are considered to be a more robust model prediction.

Table 2. Values normalized to the width of the unpolarized distribution function are listed in Table 3.

Future measurements of azimuthal moment as a function of P_T in different bins in x, z, and Q^2 combined with measurements of azimuthal moments of the unpolarized cross section proposed for `CLAS12` in case of pions [54, 55], will allow for study of the flavor dependence of transverse momentum distributions. These measurements will provide access to widths in transverse momentum of different underlying partonic distributions. Measurements with kaons will provide important independent information on width of different partonic distributions giving rise to corresponding azimuthal moments.

Studies of P_T-dependences of hadron multiplicities in a large range of kinematic variables (x_B, Q^2, z, $P_\perp$, and ϕ) with unpolarized targets, in addition, will provide important input for the polarized measurements in order to perform a P_T-dependent flavor decomposition using double spin asymmetries [55, 56].

1.3 Data on Unpolarized Azimuthal Moments

Data on azimuthal distribution in SIDIS are available from EMC experiments at CERN [57, 58], the E665 Fermilab experiment [59], and the ZEUS experiment at DESY [60, 61]. The data from ZEUS with average Q^2 value, $\langle Q^2 \rangle \simeq 750$ GeV^2, is dominated by the perturbative contribution. In order to highlight the effect of the non perturbative contributions to the $\cos 2\phi$ moment (Boer–Mulders and higher twist), one has to probe the kinematical region corresponding to $P_T < 1$ GeV and Q^2 of order of few GeV^2, such as HERMES, COMPASS, and JLAb facilities, where the gluon emission is quite irrelevant. So far the azimuthal moments were measured only for pions and charged hadrons. Data for positive pions is available from CLAS [62] and in limited range of transverse momenta from Hall-C [63]. Both COMPASS[64] and HERMES [65] presented preliminary measurements of the $\cos 2\phi$ moments for positive and negative hadrons for hydrogen and deuterium targets, indicating that the Boer-Mulders effect may be more significant than anticipated (see Fig.5).

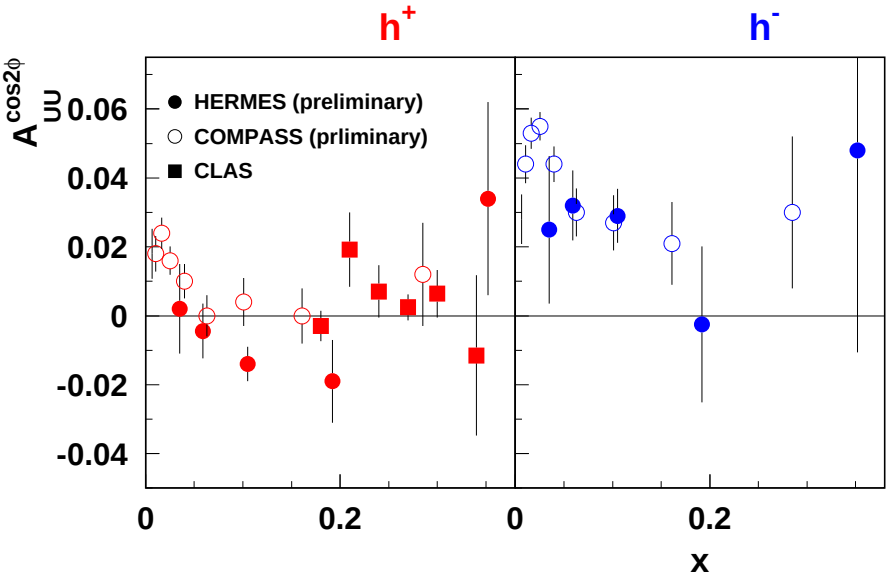

Figure 5: Preliminary measurements of the $\cos 2\phi$ moment from HERMES [65] and COMPASS[64] for positive and negative hadrons. Filled squares show the CLAS measurement for π^+ at 5.7 GeV [62].

The existing data on pions, however, are affected by large uncertainties and do not allow for drawing definite conclusions about the magnitude and the shape of the asymmetry. One of the main sources of uncertainties for pions is the fraction of pions coming from vector meson decays. Since the Collins asymmetry has a significant dependence on the type of a produced hadron, pions produced from rho decays will have very different moments compared to direct pions. This makes measurements with kaons, which have a much smaller contribution from

vector meson production, very import in understanding the underlying dynamics of the part of measured asymmetries due to Collins fragmentation mechanism.

The goal of our proposed experiment is to gather a data set on kaon SIDIS in the region $0.1 \leq x \leq 0.8$, $0 \leq P_T \leq 1.2$, and $0.2 \leq z \leq 0.8$. Global analysis of the data combined with polarized target data [55] will allow extraction of u and d-quark TMDs.

2 Experimental details

2.1 CLAS12

The proposed experiment will use the upgraded CLAS12 spectrometer with two sectors of the low threshold Cherenkov counter replaced by proximity RICH detectors. We will run at the standard magnetic field. Running conditions will be similar to an already approved CLAS12 proposal [34] for electroproduction studies with unpolarized hydrogen and deuterium targets. The central tracker will also be used for coincident detection of protons and pions. The solenoid for the central tracker is also used simultaneously to provide the magnetic field for the polarized target. Additional details on CLAS12 can be found in the document provided as an appendix to all CLAS12 proposals.

2.2 CLAS12 Particle Identification

In the baseline design of CLAS12, particle identification in the forward detector is obtained by using the high threshold Cerenkov counter (HTCC), the low threshold Cerenkov counter (LTCC) and the Time-of-flight scintillator arrays (TOF). In the $2.5-5$ GeV/c momentum region, the π/K separation relies only on the LTCC performance. Moreover, in the $4-8$ GeV/c momentum region it is not possible to separate protons from kaons. Considering that at 12 GeV for semi-inclusive processes, the K/π ratio is of the order of $10-15\%$ and assuming a pion detection inefficiency for the LTCC of 10%, then the π/K rejection factor is $1:1$. In general, this PID system is well matched to requirements of the main physics program at 12 GeV. However there are some physics reactions of high interest, such as the one covered by this proposal, that cannot be easily accessed without better PID, especially for charged kaon detection. A RICH detector, to be installed in place of the low threshold Cerenkov counter, will significantly improve the CLAS12 particle identification overcoming the limitations mentioned above.

2.2.1 CLAS12 RICH detector

A proximity focusing RICH similar to the one operating in Hall A at Jefferson Lab [66, 67] and successfully working during the hyper-nuclear spectroscopy experiment [68], may represent an adequate choice to fulfill our requirements. Presently, we didn't take into account other possibilities, such as an aerogel RICH, due to the higher costs and additional technical constraints. A proximity focusing RICH detector will allow us a good separation of $\pi/K/p$ in the $2.5-5$ GeV/c momentum region, as demonstrated later on and, in addition, replacing part or full LTCC will not have any impact on the baseline design of CLAS12. Moreover, replacing LTCC with RICH has an advantage that it can be done module by module without interfering with detector construction of CLAS12 operations. In Fig. 6 a schematic layout of the proximity focusing RICH is shown. In the RICH operating in Hall A the photons are produced by over threshold particles in the liquid freon C_6F_{14} with a refractive index of 1.28 and thickness of 15 mm. Then they refract on a quartz window of 5 mm and diverge in a 160 mm proximity gap, filled by CH_4. Eventually they are converted to electrons by a thin layer of CsI (300 nm) deposited on five pad planes that represent the cathode of a Multi-wire

Proportional Chamber. The induced charge of the electric avalanche is readout on each pad by a sample and hold analogically multiplexed front-end electronics. Spatial information is obtained from the segmented pads, whose size is $8 \times 8.4\ mm^2$. One of the most important

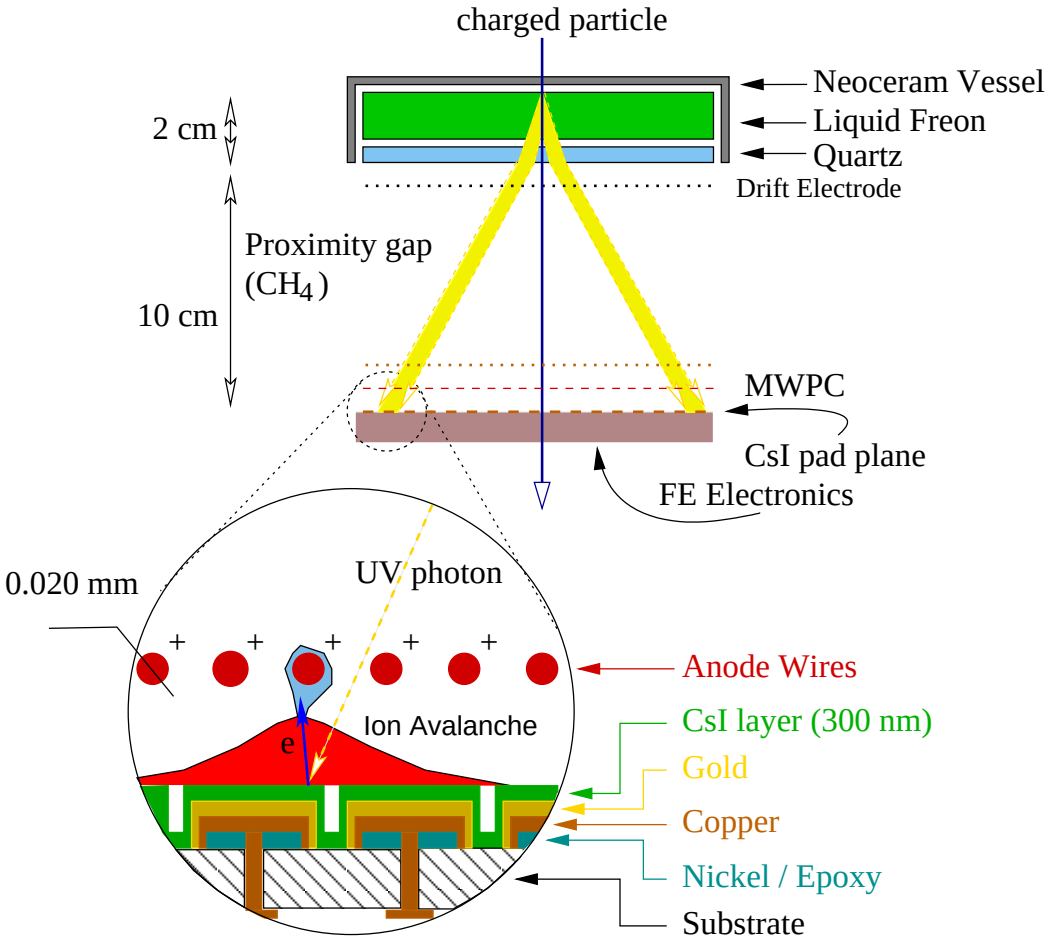

Figure 6: Schematic layout and working principle of the freon CsI proximity focusing RICH.

aspects of the proximity focusing fluorocarbon/CsI RICH detector is represented by the deposition of a layer of photo-converted material (CsI) on the pad plane. This is obtained by means of the evaporation of a pure CsI powder or crystals in a high vacuum chamber. The INFN Rome group has built, installed, and operated at JLab an evaporation chamber for large area pad (up to about 650 x 650 mm^2). A quantum efficiency (QE) online measurement system has also been integrated into the evaporation chamber. A typical measured QE is of the order of $20 - 25$ %.

Preliminary Monte Carlo studies based on GEANT3 [69] has been performed in order to optimize all the components of the detector: radiator thickness, gap length, and radiator type. The main output parameter will be the mean error on Cerenkov angle reconstruction of kaons and pions $\sigma_{K-\pi}$.

Assuming particles uniformly distributed in the phase space, results obtained for kaon-proton and kaon-pion separation versus the particle momentum are shown in Fig 7 for two

different radiators, C_5F_{12} and C_6F_{14}, respectively. In the plots the points refer to the Monte Carlo simulation while the curves are analytical functions. As we can see for the C_6F_{14} the $\sigma_{K-\pi}$ and σ_{K-p} are ~ 1 mrad larger than for the C_5F_{12} thus the use of the latter is mandatory. The disadvantage in using the freon C_5F_{12} is its need for cooling because it evaporates at 29° Celsius at standard temperature and pressure. In the simulation, the dimensions of the

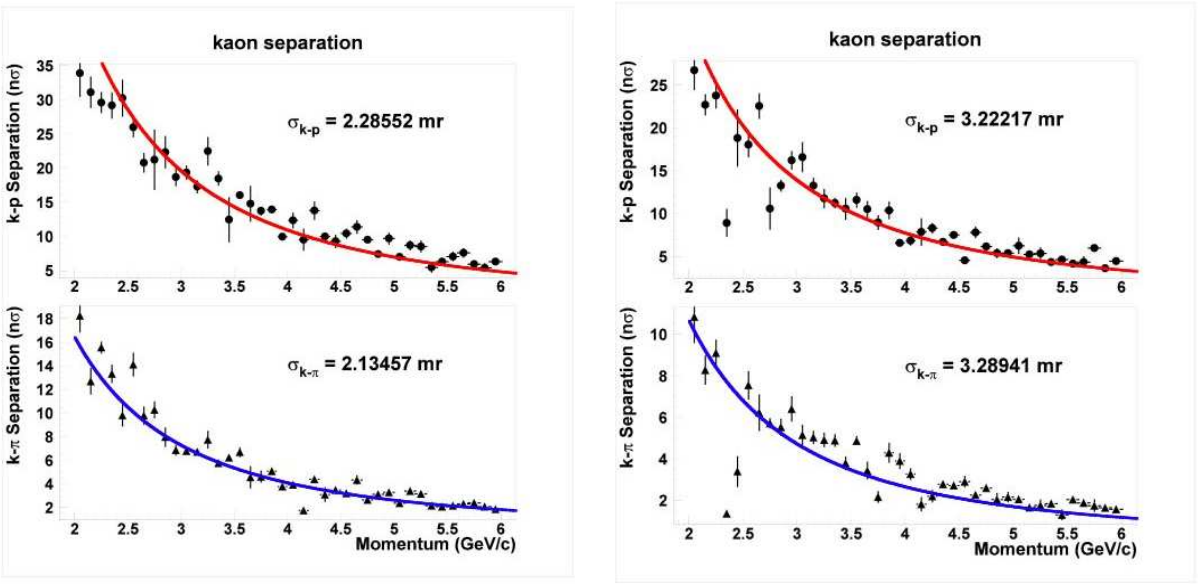

Figure 7: Left: Kaon-proton separation (upper plots) and kaon-pion separation (lower plots) versus the particle momentum for C_5F_{12}. The points refer to the Monte Carlo simulation while the curves are analytical functions. Right: Kaon-proton separation (upper plot) and kaon-pion separation (lower plot) versus the particle momentum for C_6F_{14}. The points refer to the Monte Carlo simulation while the curves are analytical functions.

radiator thickness and the gap length as well as the pad/pixel size of the photon detector have been varied in order to find the optimal combination which gives the smaller reconstruction error in the Cerenkov angle. It has been found that a freon thickness of ~ 3 cm, a gap length of ~ 80 cm and a pad size less than 1 cm minimize the $\sigma_{K-\pi}$ value. Finally, to determine the best photon detector size, pions, kaons, and protons have been generated at the LTCC-RICH entrance window according to realistic phase space distributions. The positions at the detector level of all photons generated in the radiator has been studied for a radiator polar angle acceptance of $5° - 30°$. In Fig. 8 left, the black dots are the charged particle positions at the RICH entrance (the envelope is the radiator). The contour lines are the positions at the detector level of all photons generated in the radiator (different colors refer to different intensity) while the large arc is the detector surface (photons outside of there are not detected). Our final results for the mean error on the kaon Cerenkov angle reconstruction are shown in Fig. 8 (Right). We can achieve a 4σ $K-\pi$ separation at 5 GeV/c. Therefore, we will have 80% kaon detection efficiency with 1:1000 rejection factor (or 95% with 1:100 rejection factor). This study was performed for a single sector of CLAS12, with a radiator size $\leq 4m^2$ and a detector size of $\sim 14m^2$. For six sectors, the radiator size will be $\leq 24m^2$ while the detector size of $\sim 40m^2$. The total radiation thickness of the proposed RICH is

Table 4: Radiation lengths corresponding to the different parts of the RICH detector.

	Thickness (cm)	$X_0\%$
Entrance window		
Al	0.05	0.5
Rohacell51	5	2
Al	0.05	0.5
Radiator		
Neoceram	0.4	3
C_6F_{14}	3	15
Quartz	0.5	4
Gap		
CH_4	80	0.001
Photon Detector		
Pad NEMAG10	0.08	0.4
or		
GEM chamber	1	0.6

of the order of 30% X_0. In Table 4, the radiation lengths corresponding to different parts of the RICH detector are reported. A very preliminary cost estimate has been evaluated, based on the cost of the Hall A RICH detector. Taking into consideration the replacement of two adjacent LTCC sectors, it is found to be of the order of \$2.5 M. The crucial part to be funded is the liquid radiator C_5F_{12} for which a \$0.8 M cost has been estimated (for the total quantity needed we have considered 5 times the volume of two sectors which is $\sim$ 250 l). Detailed information about the proposed RICH, its cost and parameters can be found in Ref. [70].

2.2.2 Kaon Identification with CLAS12 with TOF, LTCC and HTCC

A simulation was performed to study kinematic dependences of kaons detected using the time-of-flight scintillator arrays (TOF) at low momenta ($P < 2.5$ GeV) and the high threshold Cerenkov counter at high kaon momenta ($P > 5$ GeV), assuming very high efficiency of the HTCC for pion detection. The relevant kinematic variables for semi-inclusive DIS are the x, y, z, and the hadron transverse momentum with respect to the virtual photon P_T. While detection (identification) of kaons even in limited momentum range ($P < 2.5$ GeV and $P > 5$ GeV) will still allow a full coverage over the most accessible kinematics (see Fig.9) the statistics will be significantly less and distributions will be distorted. This is better seen for the the z and P_T-dependences of kaons, which are the most sensitive variables to the kaon momentum. The sectors of CLAS12 with no RICH will still provide data valuable for kaon studies, but data from sectors covered by RICH will be very important to use them efficiently.

2.2.3 Advantages of the RICH

The best solution to improve K^+ and K^- identification and increase the statistics ($\sim$ a factor of 3) will be complementing the PID system of forward detector with a Ring Imaging

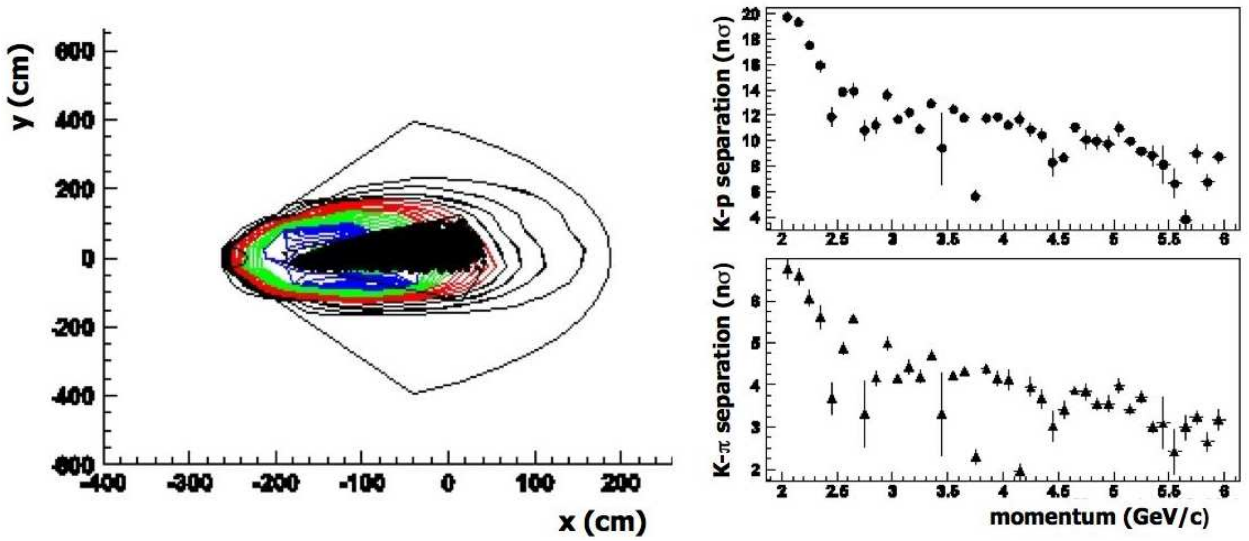

Figure 8: Left: Contour lines represent positions at the detector level of all photons generated in the radiator for a polar angle acceptance of $5^\circ - 30^\circ$. The black dots are the charged particle positions at RICH entrance; the large arc is the detector surface. x/y are not to scale. Right: Kaon-proton separation (upper plot) and kaon-pion separation (lower plot) versus the particle momentum for C_5F_{12} and a radiator polar angle acceptance of $5^\circ - 30^\circ$.

Cerenkov counter.

The time of flight can separate between kaons and protons for momenta up to 4 GeV/c. The kaon to proton ratio obtained from PEPSI Monte-Carlo is shown in Fig. 10 in the region where time of flight is not helpful. The number of proton is at least twice the number of kaons making the argument for a RICH detector even stronger.

In addition to much needed PID for kaons at momenta $P > 2.5$ GeV, RICH will help to reduce accidental in high luminosity runs, when particles from different beam buckets can mix. In Fig. 11 leakage of protons (left graph) and pions (right graph) from different beam buckets into kaons is illustrated. At high luminosities, protons and pions that get produced at high rates will leak into the kaon sample and measuring on TOF will not be enough to separate them.

2.3 The dual target

We propose to use a collinear, dual-cell target containing deuterium (for the primary measurements of multiplicities and the extraction of the shape of strange PDF) and hydrogen (for fragmentation function measurements on proton). The dual-cell target will be similar in design to the one used for the CLAS measurements of G_M^n [71] during the E5 running period. A conceptual drawing of the target is shown in Figure 12. Each of the cells containing liquid will be 2 cm in length with a 1.0 cm gap in between. The length of the cells is designed to fit within the current design of the CLAS12 silicon vertex tracker. To measure effects due to different target positions, we will collect data with the targets in opposite cells from the default configuration.

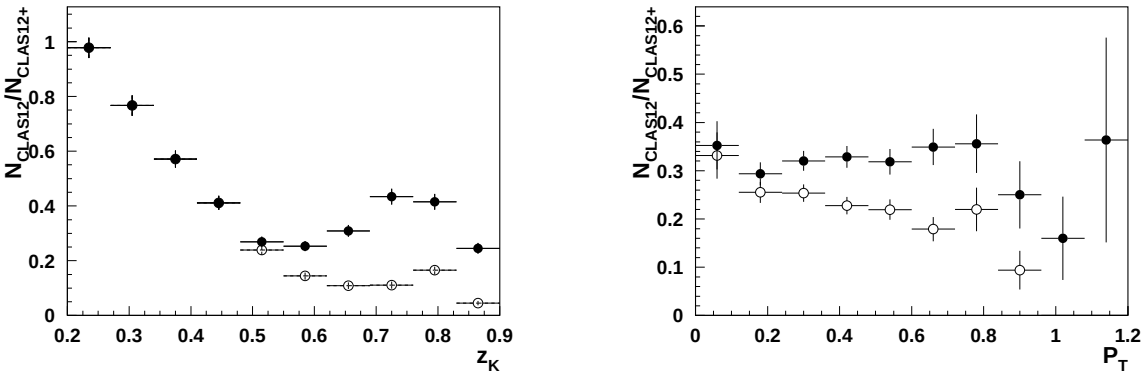

Figure 9: Relative gain of kaons with CLAS12 (with RICH) compared to the base CLAS12. The open circles assume only Kaons detected by TOF ($P < 2.5$ GeV), filled circles include both TOF and HTCC ($P > 5$ GeV). The left plot shows the z dependence while the right one shows the P_T distribution.

2.4 The data set and analysis

The expected kinematic coverage from the proposed experiment with 11 GeV beam and CLAS12 in the DIS region is shown in Fig.13. This will constitute a substantial increase over the existing Jefferson Lab data in both x and Q^2 (maximum Q^2 of 5 GeV^2 and x between 0.2 and 0.6), while the precision of the expected data will be far superior to existing DIS experiments from other labs.

2.4.1 The unpolarized data set and analysis

Realistic MC simulations are crucial for separation of different contributions to $\cos\phi$ and $\cos 2\phi$ azimuthal moments arising from higher twists, both kinematical [37] and dynamical [72, 73, 74, 75], radiative corrections [76, 77] and in particular from the detector acceptance. The CLAS12 FAST-MC program was used to simulate the physics events and study the extraction of azimuthal moments and acceptance corrections.

The SIDIS cross section assuming Gaussian $k_\perp$ and $p_\perp$ dependence, both for parton densities and fragmentation functions the cross section including only kinematic HT to the lowest order in P_T/Q is given by:

$$\frac{d^5\sigma^{\ell p\to\ell h X}}{dx_{_B}\,dQ^2\,dz_h\,d^2\mathbf{P}_T} \simeq \sum_q \frac{2\pi\alpha^2 e_q^2}{Q^4}\, f_q(x_{_B})\, D_q^h(z_h)\Big[1+(1-y)^2 + \frac{4\mu_0^2(1-y)}{\mu_H^2 Q^2}(\mu_D^2+\frac{z^2\mu_0^2 P_T^2}{\mu_H^2}) - 4\,\frac{(2-y)\sqrt{1-y}\,\mu_0^2\, z_h\,|\vec{P_T}|}{\mu_H^2\, Q}\,\cos\phi_h + \frac{4\mu_0^4 z^2(1-y)P_T^2}{\mu_H^4 Q^2}\cos 2\phi_h\Big]\frac{1}{\pi\mu_H^2}\, e^{-P_T^2/\mu_H^2}\,, \qquad (28)$$

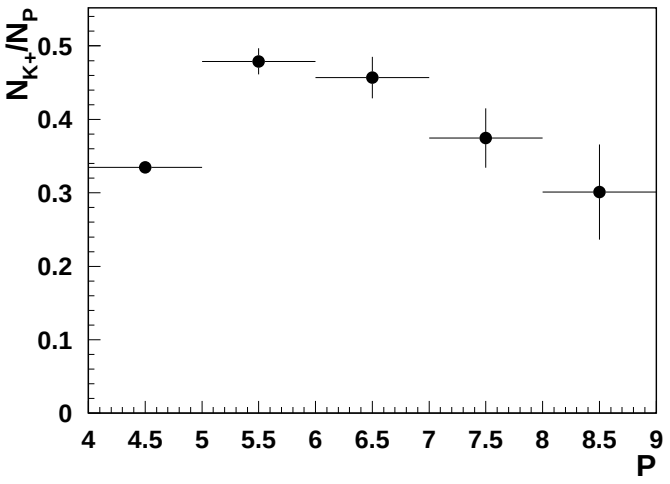

Figure 10: The ratio of K^+ to proton as a function of the momentum from CLAS12-DIS Monte-Carlo.

where $\mu_H^2 = \mu_D^2 + z_h^2\mu_0^2$ and μ_0^2 and μ_D^2 are average transverse momentum widths in distribution and fragmentation, respectively. The terms proportional to $\cos\phi_h$ and $\cos 2\phi_h$ describe the Cahn effect [37]. The Cahn effect (also Sivers effect) were included in LEPTO MC by Kotzinian [78]. The acceptance effects were studied using two alternative approaches, with different sensitivity to detector acceptance.

2.4.2 Extraction of $\cos 2\phi$, $\cos\phi$ and $\sin\phi$ moments

One of the main goals of the experiment will be to extract the $\cos 2\phi$ ($A^{\cos 2\phi}$), $\cos\phi$ ($A^{\cos\phi}$) and $\sin\phi$ ($A^{\sin\phi}$) moments as functions of Q^2, x_B, P_T, and z_h. To estimate the accuracy we will be able to achieve in the measurement of response functions, we used studies performed for pions [54], when events were generated with $A^{\cos\phi} = -0.2$, $A^{\cos 2\phi} = 0.1$, and $A^{\sin\phi} = 0.1$. These were then fed through *FastMC* to obtain the simulated detector "data". The "data" were then acceptance corrected to obtain the differential cross sections. These cross sections were then fit by a function $A(1 + Bcos2\phi + Ccos\phi)$, where A, B, and C are related to the individual moments. The fits to the cross sections for $Q^2 = 2.0$ GeV^2 are shown in Figure 14. Beam spin asymmetries are also simulated by extracting $(N^+ - N^-)/(N^+ + N^-)$ for each bin where $N^\pm$ are the number of events from $\pm$ electron helicity. These asymmetries were then fit by a function $Asin\phi/(1 + Bcos2\phi + Ccos\phi)$, where A is related to the $A^{\sin\phi}$ moment. It was demonstrated that the $A^{\cos\phi}$, $A^{\cos 2\phi}$, and $A^{\sin\phi}$ moments can be extracted over a very large kinematic range.

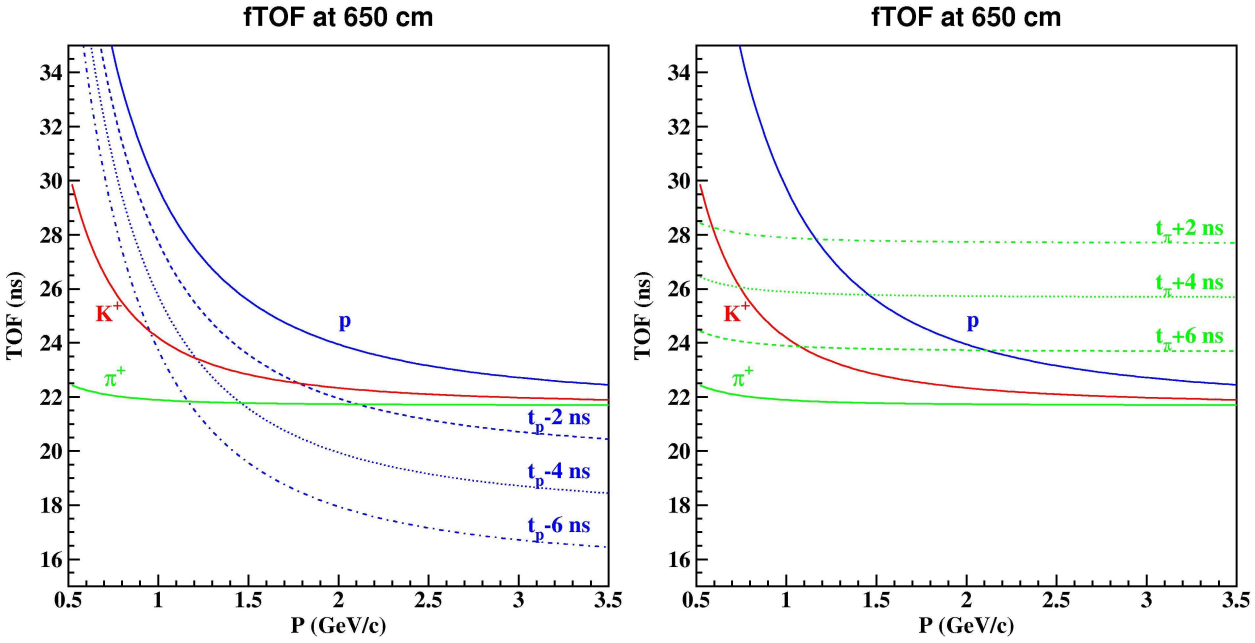

Figure 11: Time-of-flight of π^+s (green lines), K^+s (red lines), and protons (blue lines) from the target to the FTOF plane as a function momenta. On the left (right) graph - dashed line, dotted line, and dashed-dotted line correspond to protons (pions) from previous (next) beam buckets leaking into kaon samples

2.4.3 Extraction of $\cos 2\phi$, $\cos \phi$ using acceptance moments

Figure 16 shows all relevant moments extracted for the π^+ acceptance (no initial ϕ-modulation in the generated sample) and the cross section. Detailed knowledge of azimuthal moments of the acceptance allow extraction of the cross section moments from measured azimuthal moments. Using just the first two moments of the acceptance already provides a reasonable extraction of Cahn moments (see Fig.15).

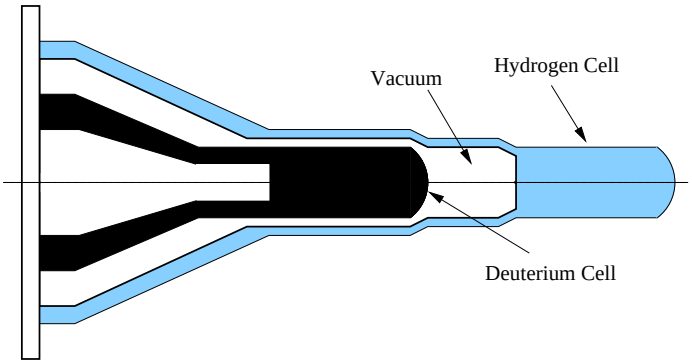

Figure 12: The conceptual design of the dual-target cell [34].

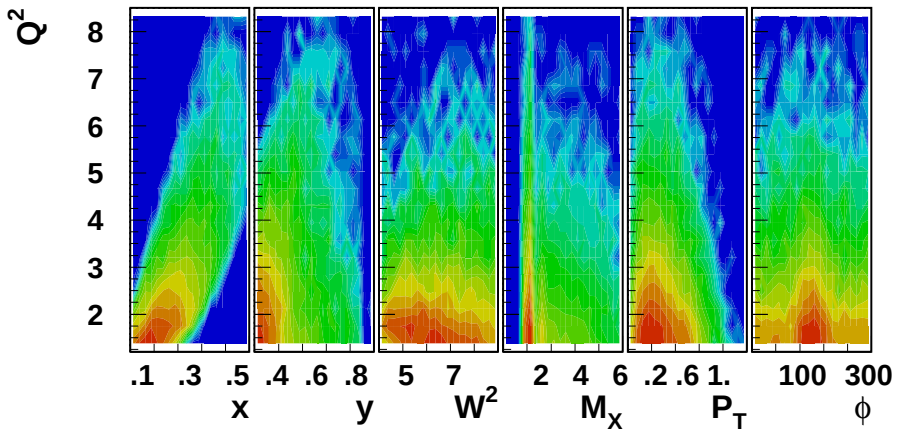

Figure 13: Kinematical coverage in the SIDIS region of the proposed experiment for eKX events.

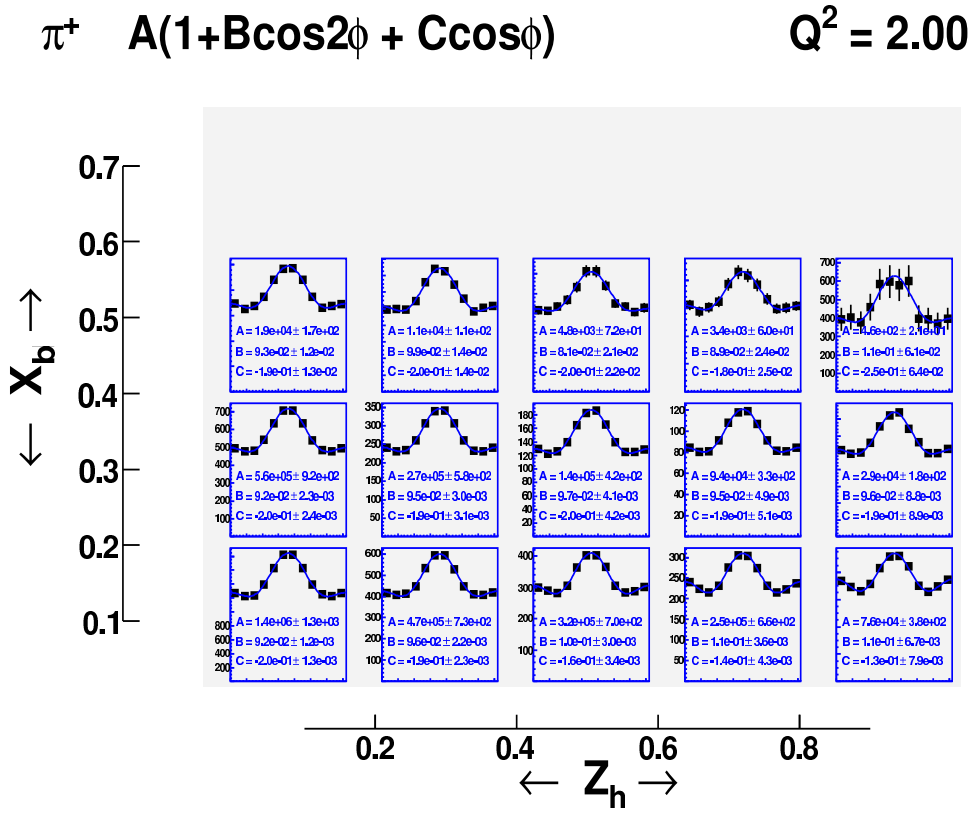

Figure 14: Simulated cross sections for the reaction $ep \rightarrow e\pi^+X$. The data were fit with the function $A(1 + Bcos2\phi + Ccos\phi)$ to obtain the parameters A, B and C

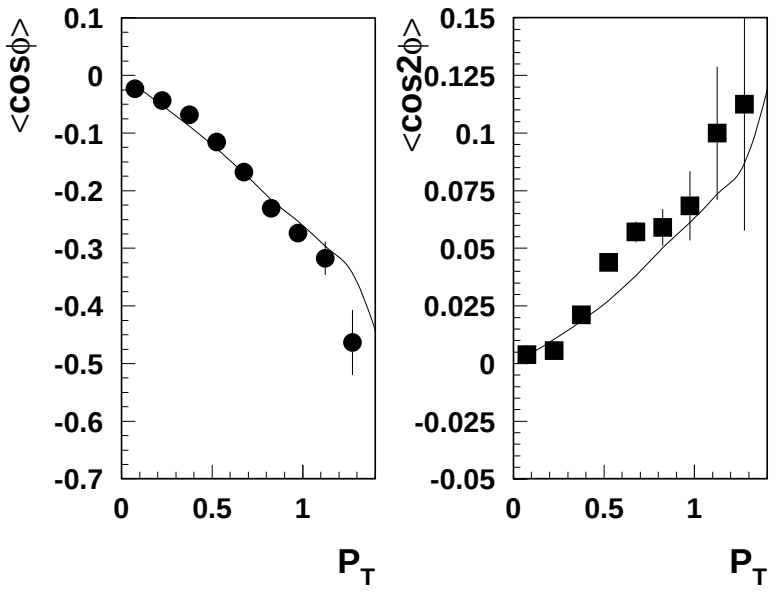

Figure 15: Extracted $< cos\phi >$ and $< cos2\phi >$ moments of the $e\pi^+X$ cross section from the MC-data (circles) compared to initial moments used as input in the PEPSI-MC (curves).

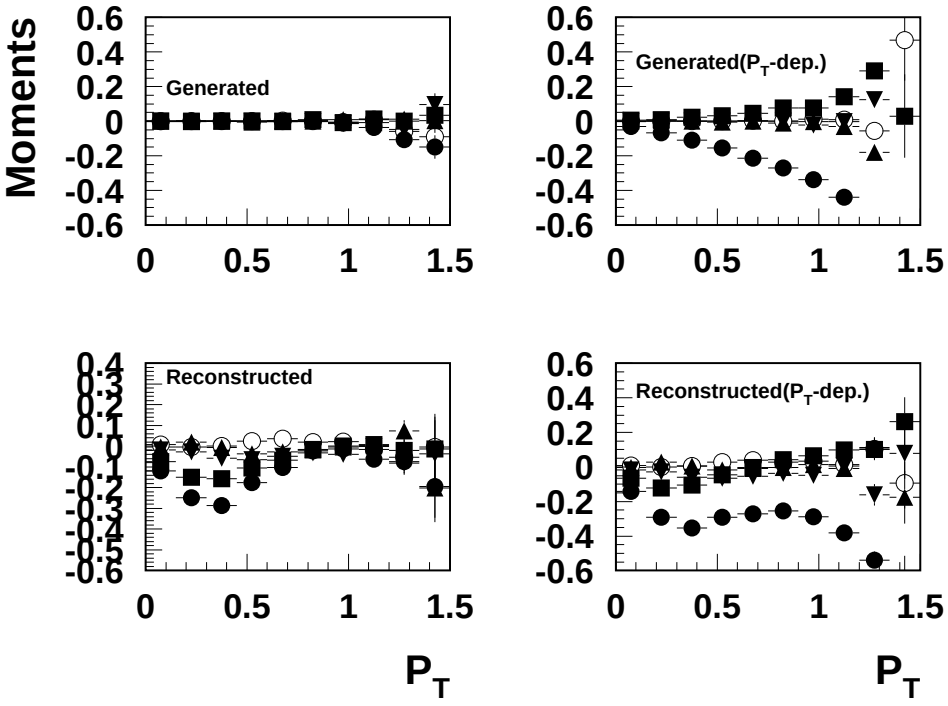

Figure 16: Extracted azimuthal moments for $e\pi^+X$ using the PEPSI-MC with (right panel) and without (left panel) account of azimuthal moments in the cross section. Circles,squares, triangles up and down are for $< cos\phi >, < cos2\phi >, < cos3\phi >, < cos4\phi >, < cos5\phi >$, respectively.

3 Expected results

3.1 Simulation

The expected number of counts and corresponding statistical errors in the following sections are based on a full simulation of inclusive and semi-inclusive inelastic scattering with the CLAS12 acceptance folded in. Events were generated with the clas12DIS generator [79]. This generator is basically an implementation of the LUND Monte Carlo package called PEPSI (Polarized Electron-Proton Scattering Interactions) [80]. It is based on polarized and unpolarized parton distribution functions and the LUND string model for hadronization, and has been tested successfully against several low-Q^2 experiments with 5.7 GeV beam at Jefferson Lab.

A fast Monte Carlo simulation program has been used to define the acceptance and resolution of the CLAS12 detector with all of the standard (base) equipment in place. The kaons were assumed identified 100% in sectors covered by CLAS12-RICH, and also at energies above 5 GeV, where the pions start to fire the High Threshold Cherekov Counter (HTCC). The events generated by clas12DIS are used as input and all particles are followed through all detector elements. The results of our simulation have been cross-checked with direct cross section calculations and a simple geometric acceptance model.

The resolution of the detector is simulated by a simple smearing function which modifies a particle's track by a random amount in momentum and angles according to a Gaussian distribution of the appropriate width. The amount of smearing follows the design specifications of the CLAS12 detector. The resolution in x_B varies between $0.01 < \sigma_x < 0.035$ and is therefore finer than our planned x bin size of 0.05 in all cases.

A full Monte Carlo simulation (GEANT-based) of CLAS12 with all resolution effects will be used to determine the effective mean x (and Q^2) for each x-bin we will use to bin our data so we can accurately extract the x-dependence of the measured asymmetries.

3.2 Statistical and systematic errors

The proposed spin asymmetry measurement is rather insensitive to uncertainties in acceptances and charge normalization. The overall statistics of kaons is, though, an order of magnitude less than for pions, with most of the relevant sources of systematic errors being the same. One of the main systematic errors affecting the extraction of the Collins moment is due to possible contamination of the single kaon sample with kaons from decays of exclusive K^* mesons. The fraction of indirect kaons, however, according to LUND studies, is significantly less than for pions (see Fig.17). The main difference from the pion production case for the background is the contribution from K^* production (e.g., $K^* \to K\pi$) and the radiative tail on exclusive Kaon production. The contributions to the systematic error from these backgrounds requires a detailed analysis once the requisite data are in hand, but experience with pion data from CLAS at 6 GeV show that one can avoid most of them by judicious choice of kinematic cuts.

Other sources of systematic errors include the longitudinal to transverse photo absorption cross section ratio, $R(x, Q^2)$ and the beam polarization (for $\sin\phi$). The main sources of systematic errors in measurements of azimuthal asymmetries are listed in the Table 5. These

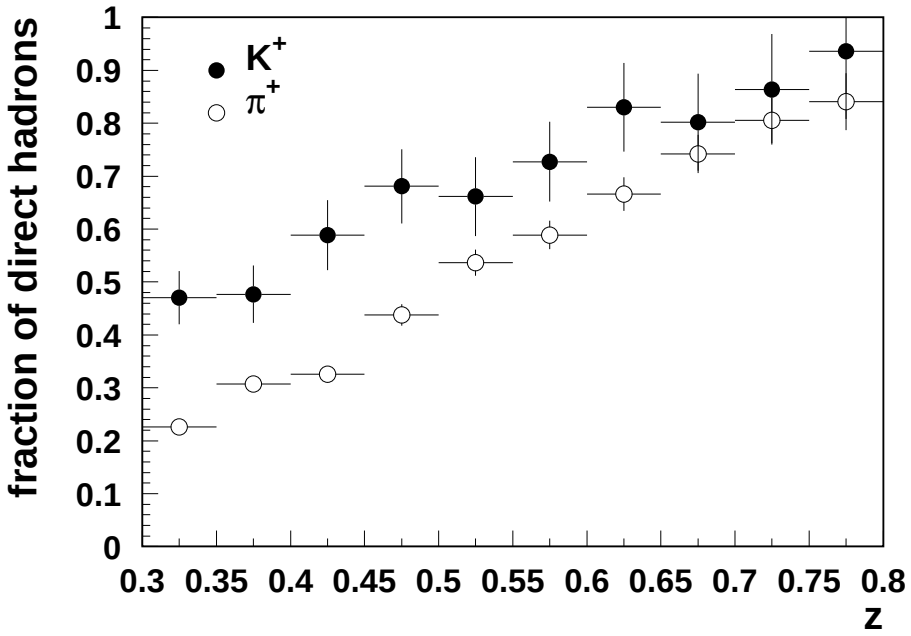

Figure 17: Fractions of direct (with a parent defined as "string") kaons and pions from PEPSI MC for ehX events.

Table 5: Uncertainties for asymmetry measurements.

Item	$A_{UU}^{\cos 2\phi}$	$A_{UU}^{\cos \phi}$	$A_{LU}^{\sin \phi}$
beam polarization	-	-	3%
acceptance corrections	4%	4%	2%
radiative corrections	3%	3%	3%
fitting procedure	4%	4%	3%

errors are all scale errors, so they are proportional to the size of the measured asymmetry.

Studies of other sources of systematics, related to physics background, including target fragmentation, semi-exclusive processes, exclusive vector meson contributions, and higher twist require the data of this measurement.

We based our predicted statistical errors in the following sections on the assumption of running 54 days on a hydrogen and deuterium [34]. For our estimate of the total systematic error, we have added the systematic errors from the various contributions discussed in the previous Section in quadrature. They are listed in Table 5.

3.2.1 Exclusive production of K* and GPDs

While understanding of K*–production is important for extracting the kaon moments studied in the present proposal, it is also interesting in its own right, as the exclusive $K^*\Lambda$ channel provides access to the Generalized Parton Distributions (GPDs) associated with the $p \to \Lambda$ transition. A QCD factorization theorem [81] states that in the limit $Q^2 \to \infty$ the meson is predominantly produced in configurations of small transverse size $\sim 1/Q$, and the longitudinal cross section can be expressed in terms of the GPDs and the distribution amplitude of the produced meson. In the Q^2 range covered by JLab one expects significant finite–size ("higher–twist") corrections to the asymptotic production mechanism, making it difficult to interpret absolute cross sections within the GPD formalism [82]. The focus here is on the analysis of cross section ratios, which are less sensitive to finite–size effects and can be compared with GPD–based expressions already at $Q^2 \sim$ few GeV^2 [83].

Figure 18 shows a simple prediction for the ratio of exclusive K^* and ρ^+ production, based on $SU(3)$ flavor symmetry and approximation of the GPDs by the "usual" parton densities; estimates based on more sophisticated GPD models were presented in Ref. [84]. Analysis of the Q^2–dependence of the measured ratio will serve as a test of the expected early scaling. The observed limiting (Q^2–independent) value can then be compared with the theoretical predictions and provide an interesting test of $SU(3)$ flavor symmetry and present GPD models. The K^*/ρ^+ ratio addressed here is particularly useful for this purpose because (a) both channels involve non-singlet quark GPDs, eliminating the uncertainty associated with modeling gluon and singlet quark exchange in ρ^0 and ϕ production; (b) the final–state masses of the produced meson/baryon systems are similar, reducing $SU(3)$ breaking effects resulting from kinematic corrections in the cross section ratio; (c) the longitudinal cross section (for which the QCD factorization theorem applies) can be extracted by analyzing the decay of the vector meson and relying on s–channel helicity conservation, eliminating the need for Rosenbluth separation as is necessary in pseudoscalar (π, K) meson production.

It is important to note that detection of exclusive K^*s, unlike the case with exclusive kaons, where the missing mass technique could be used, will require kaon identification over the full kinematic range, which could be provided only by the RICH detector.

3.3 Results

The proposed experiment will simultaneously collect data on $p, d(\vec{e}, e'h)$, including kaons and pions. The charged kaons will be detected in the forward spectrometer and the central tracker of CLAS12 in coincidence with the scattered electrons and identified by the CLAS12-RICH detector. The following predicted results were obtained with a full simulation of the hadronization process [80] and the acceptance of CLAS12 for all particles.

The expected counts of kaons in different kinematic bins for the hydrogen and deuteron targets for each of the kaon charges were calculated using the PEPSI-MC kaon to pion ratios (Fig.19).

3.3.1 Projected results for unpolarized moments

The precision measurement of the Boer-Mulders asymmetry requires subtraction of all contributions to the $\cos 2\phi$ moment discussed above. All contributions, including the Cahn

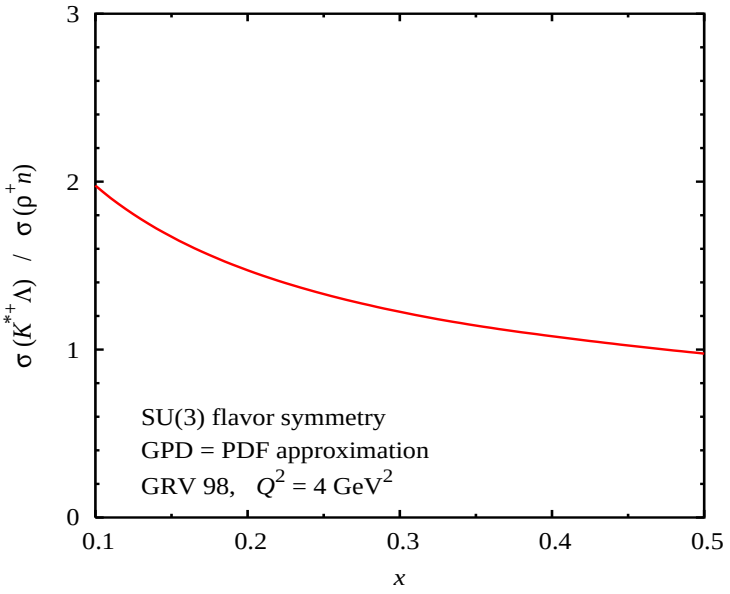

Figure 18: Theoretical estimate of the longitudinal cross section ratio for exclusive $K^*\Lambda$ and $\rho^+ n$ production, $\sigma(\gamma_L^* p \to K^*\Lambda)/\sigma(\gamma_L^* p \to \rho^+ n)$, based on $SU(3)$ flavor symmetry for the GPDs and vector meson distribution amplitudes, and approximation of the GPDs by the "usual" quark densities. The results for the ratio in this approximation are close to those obtained with more sophisticated GPD models [84].

and Berger terms as well as the perturbative and radiative contributions to first order, are expected to be "flavor blind", i.e. are the same for negative and positive kaons. The check performed with the $\cos\phi$ moment can serve as a test for that. Contributions to $\cos\phi$ moment are also related to contributions to $\cos 2\phi$ and their extraction will provide an additional check for the background contributions to $\cos 2\phi$ being under control. Extraction of $\cos\phi$ and $\cos 2\phi$ moments for kaons will also provide additional to pion measurements [54], information on widths of k_T distributions, and their flavor dependence. The difference of the $\cos 2\phi$ moments for K^+ and K^- from π^+ and π^- will provide important information about sea orbital structure, described by corresponding Collins functions. Simultaneous measurement of the $\cos 2\phi$ and $\sin 2\phi$ moment of the cross section will provide independent measurements of the Collins effect, and provide complementary information to measurements of the Collins effect [20] with transversely polarized target [85] as well as direct measurements, which may be performed at BELLE [33].

Projections for some of the most important observables are shown on Figs. 20,21 for proton and deuteron targets, respectively. Measured $\cos 2\phi$ moment for charged kaons for two targets, combined with the measurements on pions [54], will allow the extraction of the Collins analyzing power ratios for pions and kaons, providing information on the polarized fragmentation function of kaons.

Proposed measurements of azimuthal asymmetries in SIDIS will measure the ratio of favored to unfavored polarized fragmentation functions for kaons provide independent to pion measurements constrains on the corresponding TMD distributions. The new data will

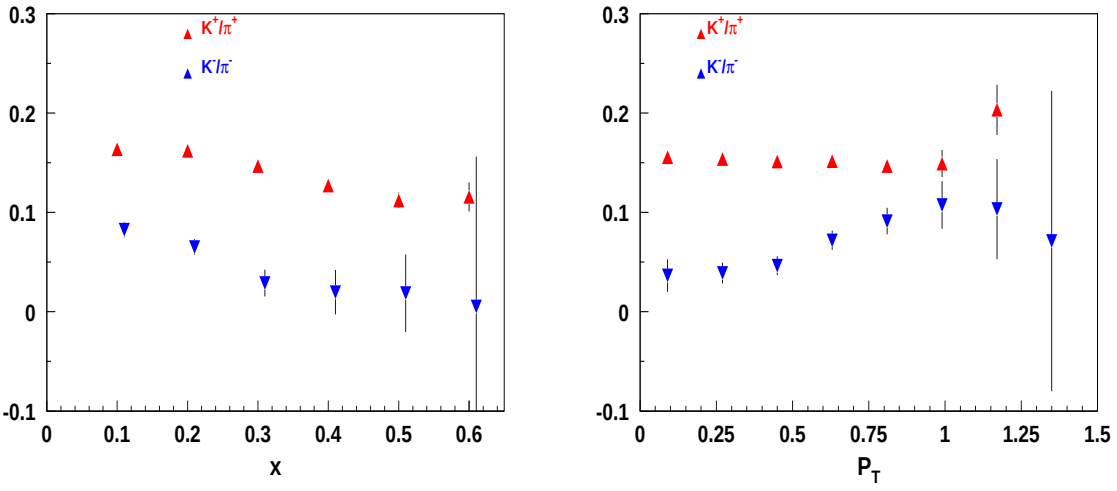

(a) (b)

Figure 19: PEPSI-Lepto predictions for x-dependence (left) and P_T-dependence of kaon pion ratios.

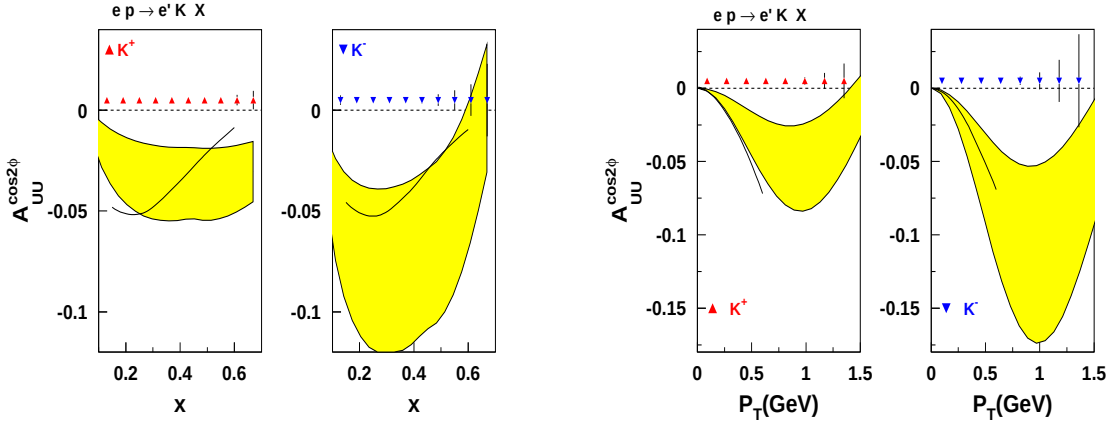

(a) (b)

Figure 20: The $\cos 2\phi$ moment for kaons as a function of x (left) and P_T (right) for proton target at 11 GeV from 80 days of CLAS12 running. The band corresponds to set-I of Ref.[46] with Boer-Mulders function extracted [86] from the Drell-Yan data [87]. The Collins fragmentation function was approximated using the chiral limit. The black curve is from Ref. [45], with Collins function from parametrization [47] based on the e^+e^- and SIDIS data.

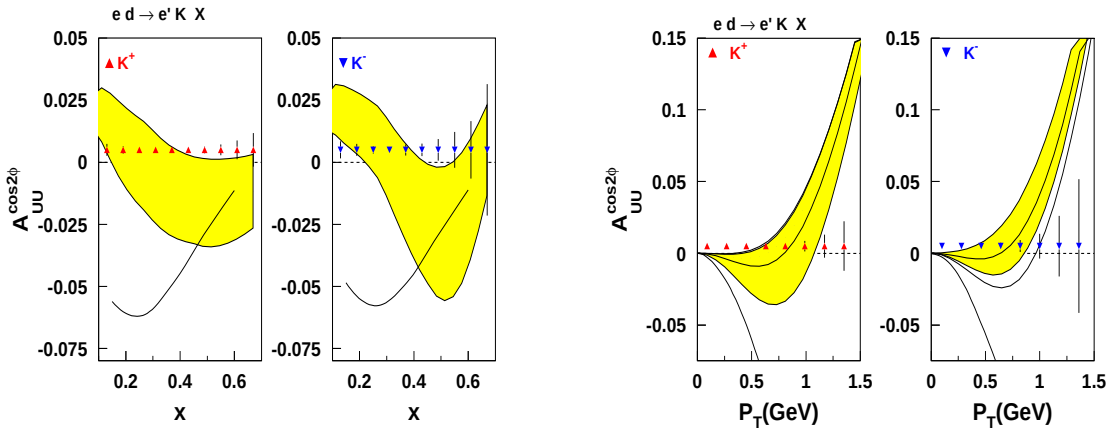

Figure 21: The $\cos 2\phi$ moment for kaons as a function of x (left) and P_T (right) for deuteron target at 11 GeV from 80 days of CLAS12 running. Curves are calculated using assumptions for Collins fragmentation function discussed above.

also allow a more precise test of the factorization ansatz and the investigation of the Q^2 dependence of $\cos 2\phi$, $\cos\phi$, and $\sin\phi$ asymmetries. This will enable us to study the leading-twist and higher-twist nature of the corresponding observables [37, 88, 3].

Measurement of the P_T dependence of the Boer-Mulders-asymmetry will also allow for checking of the high P_T predictions [12, 89, 42] to study the transition from a non-perturbative to a perturbative description. Both $\cos 2\phi$ and $\sin 2\phi$ asymmetries for semi-inclusive deep inelastic scattering in the kinematic regions of `CLAS12` are predicted to be significant (a few percent on average) and tending to be larger in the large-x and large-z region.

The combined analysis of the future `CLAS12` data on $\langle\cos 2\phi\rangle$ and of the previous HERMES measurements in the high-Q^2 domain (where higher-twist effects are less significant) will provide information on the Boer-Mulders function, shedding light on the correlations between transverse spin and transverse momenta of quarks.

At lower x, this very large data set allows us to further subdivide the data into bins in P_T and z. Once in hand, these data will be combined with CLAS12 data on pions and existing SIDIS data from HERMES, COMPASS and RHIC for a full NLO analysis.

Measured azimuthal asymmetries for kaons in a large range of kinematic variables (x_B, Q^2, z, $P_\perp$ and ϕ) combined with measurements with polarized target measurements and data for pions [55], will provide detailed information on flavor and polarization dependence of transverse momentum distributions of quarks in valence region and in particular on the x_B and k_T dependence of leading TMD parton distribution functions. Measurements of spin and azimuthal asymmetries across a wide range of x, z, Q^2, and P_T would allow to perform detailed tests of QCD dynamics in valence region.

Time	Activity
2 days	Commissioning: Empty target, interchange of targets
54 days	Production data taking on proton and deuterium (50% with reversed field)

Table 6: Requested beam time broken down by activity.

4 Summary and Request

Understanding of spin-orbit correlations, together with independent measurements related to the spin and orbital angular momentum of the quarks, will help to construct a more complete picture of the nucleon in terms of elementary quarks and gluons going beyond the simple collinear partonic representation. The proposed set of measurements on unpolarized proton and deuteron targets will yield a comprehensive set of azimuthal moments in spin-dependent and independent SIDIS providing access to corresponding distribution and fragmentation functions in a wide range of x, Q^2, z, and P_T. Our data, combined with the data from HERMES, COMPASS, and BELLE, will provide independent (complementary to e^+/e^-) measurement of polarized kaon Collins fragmentation function and will allow a study complementary to pion SIDIS study of leading twist TMD parton distribution $h_1^\perp(x, k_T)$.

In addition, the proposed experiment will yield data on single beam spin asymmetries in SIDIS, which can provide constraints on the higher-twist nucleon structure functions. As a by-product, the experiment will also provide interesting data on the exclusive cross section ratio $K * Lambda/rho^+n$, which can be interpreted within the GPD formalism.

To achieve this goal, we request a total of 56 days of beam time with an 11 GeV electron beam in Hall B. We assume the same target configuration as an already approved experiment on measurement of the neutron magnetic form-factors [34]. The breakdown of this beam time is shown in Table 6. The number of days requested was chosen to allow a statistically significant measurement of the T-odd distribution and fragmentation functions.

We want to conclude by noting that while this proposed experiments requires a substantial commitment of beam time (56 days total), we will simultaneously take data with an already approved experiment to study the neutron magnetic form-factor [34].

Appendix-I

Isospin and charge-conjugation relations imply for "favored" functions

$$D_1^{u\to\pi^+} = D_1^{\bar{d}\to\pi^+} = D_1^{d\to\pi^-} = D_1^{\bar{u}\to\pi^-}, \equiv D_1^{\rm f} \tag{29}$$

$$D_1^{u\to K^+} = D_1^{\bar{u}\to K^-}, \equiv D_1^{\rm fd} \tag{30}$$

$$D_1^{\bar{s}\to K^+} = D_1^{s\to K^-} \equiv D_1^{\rm f'} \tag{31}$$

for the "unfavored" functions

$$D_1^{\bar{u}\to\pi^+} = D_1^{d\to\pi^+} = D_1^{\bar{d}\to\pi^-} = D_1^{u\to\pi^-} \equiv D_1^{\rm d}, \tag{32}$$

$$D_1^{s\to\pi^+} = D_1^{\bar{s}\to\pi^+} = D_1^{s\to\pi^-} = D_1^{\bar{s}\to\pi^-} \equiv D_1^{\rm df}, \tag{33}$$

$$D_1^{\bar{u}\to K^+} = D_1^{\bar{d}\to K^+} = D_1^{d\to K^+} = D_1^{\bar{d}\to K^-} = D_1^{d\to K^-} = D_1^{u\to K^-} \equiv D_1^{\rm dd}, \tag{34}$$

$$D_1^{s\to K^+} = D_1^{\bar{s}\to K^-} \equiv D_1^{\rm d'}. \tag{35}$$

There are in principle seven independent functions. Further assumption could be to set $D_1^{\rm f'} = D_1^{\rm f}$ and $D_1^{\rm d'} = D_1^{\rm d}$, leaving five independent functions.

For the Collins function, one can consider the Schäfer–Teryaev sum rule [90], which states that

$$\sum_h \int_0^1 dz H_{1(q\to h)}^{\perp(1)}(z) = 0 \qquad \text{with} \qquad H_1^{\perp(1)}(z) = \pi z^2 \int_0^\infty dk_T^2 \, \frac{\boldsymbol{k}_T^2}{2M_h^2} \, H_1^\perp(z, k_T^2). \tag{36}$$

Assuming that the sum rule holds in a strong sense, i.e., for pions and kaons separately and at the integrand level, for each value of z and k_T. For pions, using also it follows that

$$H_{1(u\to\pi^+)}^\perp = H_{1(\bar{d}\to\pi^+)}^\perp = H_{1(d\to\pi^-)}^\perp = H_{1(\bar{u}\to\pi^-)}^\perp \equiv H_1^{\perp\rm f} \tag{37}$$

$$H_{1(u\to\pi^-)}^\perp = H_{1(d\to\pi^+)}^\perp = H_{1(d\to\pi^+)}^\perp = H_{1(\bar{u}\to\pi^+)}^\perp \equiv -H_1^{\perp\rm f} \tag{38}$$

With such a "strong" interpretation of the Schäfer–Teryaev sum rule together with Eq. (33) (with D_1 replaced by $H_1^\perp$) implies

$$H_{1(s\to\pi^+)}^\perp = -H_{1(s\to\pi^-)}^\perp = H_{1(\bar{s}\to\pi^+)}^\perp = -H_{1(\bar{s}\to\pi^-)}^\perp = 0. \tag{39}$$

For kaons, the same considerations lead to the following assumptions

$$H_{1(u\to K^+)}^\perp = H_{1(\bar{u}\to K^-)}^\perp \equiv H_1^{\perp\rm fd}, \tag{40}$$

$$H_{1(u\to K^-)}^\perp = H_{1(\bar{u}\to K^+)}^\perp \equiv -H_1^{\perp\rm fd}, \tag{41}$$

$$H_{1(\bar{s}\to K^+)}^\perp = H_{1(s\to K^-)}^\perp \equiv H_1^{\perp\rm f'}, \tag{42}$$

$$H_{1(\bar{s}\to K^-)}^\perp = H_{1(s\to K^+)}^\perp \equiv -H_1^{\perp\rm f'}, \tag{43}$$

$$H_{1(d\to K^-)}^\perp = -H_{1(d\to K^+)}^\perp = H_{1(\bar{d}\to K^-)}^\perp = -H_{1(\bar{d}\to K^+)}^\perp = 0. \tag{44}$$

In total, we are left with only three independent Collins functions.

Then pion and kaon *weighted* asymmetries can be written as (using a generic chiral-odd function as an example)

$$A^{p/\pi^+}(x,y,z) = \frac{B(y)}{A(y)} \frac{\left(4\,h^u + h^{\bar{d}}\right) H_1^{\perp(1)\mathrm{f}} - \left(4\,h^{\bar{u}} + h^d\right) H_1^{\perp(1)\mathrm{f}}}{\left(4\,f_1^u + f_1^{\bar{d}}\right) D_1^{\mathrm{f}} + \left(4\,f_1^{\bar{u}} + f_1^d\right) D_1^{\mathrm{d}} + \left(f_1^s + f_1^{\bar{s}}\right) D_1^{\mathrm{df}}}, \tag{45}$$

$$A^{p/\pi^-}(x,y,z) = \frac{B(y)}{A(y)} \frac{\left(4\,h^{\bar{u}} + h^d\right) H_1^{\perp(1)\mathrm{f}} - \left(4\,h^u + h^{\bar{d}}\right) H_1^{\perp(1)\mathrm{f}}}{\left(4\,f_1^{\bar{u}} + f_1^d\right) D_1^{\mathrm{f}} + \left(4\,f_1^u + f_1^{\bar{d}}\right) D_1^{\mathrm{d}} + \left(f_1^s + f_1^{\bar{s}}\right) D_1^{\mathrm{df}}}, \tag{46}$$

$$A^{n/\pi^+}(x,y,z) = \frac{B(y)}{A(y)} \frac{\left(4\,h^d + h^{\bar{u}}\right) H_1^{\perp(1)\mathrm{f}} - \left(4\,h^{\bar{d}} + h^u\right) H_1^{\perp(1)\mathrm{f}}}{\left(4\,f_1^d + f_1^{\bar{u}}\right) D_1^{\mathrm{f}} + \left(4\,f_1^{\bar{d}} + f_1^u\right) D_1^{\mathrm{d}} + \left(f_1^s + f_1^{\bar{s}}\right) D_1^{\mathrm{df}}}, \tag{47}$$

$$A^{n/\pi^-}(x,y,z) = \frac{B(y)}{A(y)} \frac{\left(4\,h^{\bar{d}} + h^u\right) H_1^{\perp(1)\mathrm{f}} - \left(4\,h^d + h^{\bar{u}}\right) H_1^{\perp(1)\mathrm{f}}}{\left(4\,f_1^{\bar{d}} + f_1^u\right) D_1^{\mathrm{f}} + \left(4\,f_1^d + f_1^{\bar{u}}\right) D_1^{\mathrm{d}} + \left(f_1^s + f_1^{\bar{s}}\right) D_1^{\mathrm{df}}}, \tag{48}$$

$$A^{p/K^+}(x,y,z) = \frac{B(y)}{A(y)} \frac{4\left(h^u - h^{\bar{u}}\right) H_1^{\perp(1)\mathrm{fd}} - \left(h^s - h^{\bar{s}}\right) H_1^{\perp(1)\mathrm{f}'}}{4\,f_1^u\,D_1^{\mathrm{fd}} + \left(4\,f_1^{\bar{u}} + f_1^d + f_1^{\bar{d}}\right) D_1^{\mathrm{dd}} + f_1^{\bar{s}}\,D_1^{\mathrm{f}'} + f_1^s\,D_1^{\mathrm{d}'}}, \tag{49}$$

$$A^{p/K^-}(x,y,z) = \frac{B(y)}{A(y)} \frac{-4\left(h^u - h^{\bar{u}}\right) H_1^{\perp(1)\mathrm{fd}} + \left(h^s - h^{\bar{s}}\right) H_1^{\perp(1)\mathrm{f}'}}{4\,f_1^{\bar{u}}\,D_1^{\mathrm{fd}} + \left(4\,f_1^u + f_1^d + f_1^{\bar{d}}\right) D_1^{\mathrm{dd}} + f_1^s\,D_1^{\mathrm{f}'} + f_1^{\bar{s}}\,D_1^{\mathrm{d}'}}, \tag{50}$$

$$A^{n/K^+}(x,y,z) = \frac{B(y)}{A(y)} \frac{4\left(h^d - h^{\bar{d}}\right) H_1^{\perp(1)\mathrm{fd}} - \left(h^s - h^{\bar{s}}\right) H_1^{\perp(1)\mathrm{f}'}}{4\,f_1^d\,D_1^{\mathrm{fd}} + \left(4\,f_1^{\bar{d}} + f_1^u + f_1^{\bar{u}}\right) D_1^{\mathrm{dd}} + f_1^{\bar{s}}\,D_1^{\mathrm{f}'} + f_1^s\,D_1^{\mathrm{d}'}}, \tag{51}$$

$$A^{n/K^-}(x,y,z) = \frac{B(y)}{A(y)} \frac{-4\left(h^d - h^{\bar{d}}\right) H_1^{\perp(1)\mathrm{fd}} + \left(h^s - h^{\bar{s}}\right) H_1^{\perp(1)\mathrm{f}'}}{4\,f_1^{\bar{d}}\,D_1^{\mathrm{fd}} + \left(4\,f_1^d + f_1^u + f_1^{\bar{u}}\right) D_1^{\mathrm{dd}} + f_1^s\,D_1^{\mathrm{f}'} + f_1^{\bar{s}}\,D_1^{\mathrm{d}'}}, \tag{52}$$

The sums of the numerators of the π^+ and π^- and of the K^+ and K^- observables always vanish.

References

[1] European Muon, J. Ashman et al., Phys. Lett. B206 (1988) 364.

[2] P.J. Mulders and R.D. Tangerman, Nucl. Phys. B461 (1996) 197, hep-ph/9510301.

[3] A. Bacchetta et al., JHEP 02 (2007) 093, hep-ph/0611265.

[4] V. Barone, A. Drago and P.G. Ratcliffe, Phys. Rept. 359 (2002) 1, hep-ph/0104283.

[5] D.W. Sivers, Phys. Rev. D43 (1991) 261.

[6] M. Anselmino and F. Murgia, Phys. Lett. B442 (1998) 470, hep-ph/9808426.

[7] S.J. Brodsky, D.S. Hwang and I. Schmidt, Phys. Lett. B530 (2002) 99, hep-ph/0201296.

[8] J.C. Collins, Phys. Lett. B536 (2002) 43, hep-ph/0204004.

[9] X. Ji and F. Yuan, Phys. Lett. B543 (2002) 66, hep-ph/0206057.

[10] A.V. Belitsky, X. Ji and F. Yuan, Nucl. Phys. B656 (2003) 165, hep-ph/0208038.

[11] D. Boer, P.J. Mulders and F. Pijlman, Nucl. Phys. B667 (2003) 201, hep-ph/0303034.

[12] X. Ji, J. Ma and F. Yuan, Phys. Rev. D71 (2005) 034005, hep-ph/0404183.

[13] J.C. Collins and A. Metz, Phys. Rev. Lett. 93 (2004) 252001, hep-ph/0408249.

[14] X.d. Ji, J.P. Ma and F. Yuan, Nucl. Phys. B652 (2003) 383, hep-ph/0210430.

[15] S.J. Brodsky, D.S. Hwang and I. Schmidt, Nucl. Phys. B642 (2002) 344, hep-ph/0206259.

[16] J.P. Ralston and D.E. Soper, Nucl. Phys. B152 (1979) 109.

[17] C.J. Bomhof and P.J. Mulders, Nucl. Phys. B795 (2008) 409.

[18] J. Collins and J.W. Qiu, Phys. Rev. D75 (2007) 114014, 0705.2141.

[19] W. Vogelsang and F. Yuan, Phys. Rev. D76 (2007) 094013, 0708.4398.

[20] J.C. Collins, Nucl. Phys. B396 (1993) 161, hep-ph/9208213.

[21] A. Metz, Phys. Lett. B549 (2002) 139.

[22] F. Yuan, Phys. Rev. D77 (2008) 074019, 0801.3441.

[23] HERMES, A. Airapetian et al., Phys. Rev. Lett. 84 (2000) 4047, hep-ex/9910062.

[24] HERMES, A. Airapetian et al., Phys. Rev. D64 (2001) 097101, hep-ex/0104005.

[25] HERMES, A. Airapetian et al., Phys. Rev. Lett. 94 (2005) 012002, hep-ex/0408013.

[26] HERMES, A. Airapetian, (2006), hep-ex/0612059.

[27] COMPASS, V.Y. Alexakhin et al., Phys. Rev. Lett. 94 (2005) 202002, hep-ex/0503002.

[28] CLAS, H. Avakian et al., Phys. Rev. D69 (2004) 112004, hep-ex/0301005.

[29] CLAS, H. Avakian et al., AIP Conf. Proc. 792 (2005) 945, nucl-ex/0509032.

[30] STAR, J. Adams et al., Phys. Rev. Lett. 92 (2004) 171801, hep-ex/0310058.

[31] PHENIX, M. Chiu, AIP Conf. Proc. 915 (2007) 539, nucl-ex/0701031.

[32] BRAHMS, I. Arsene et al., Phys. Rev. Lett. 101 (2008) 042001, 0801.1078.

[33] Belle, K. Abe et al., Phys. Rev. Lett. 96 (2006) 232002, hep-ex/0507063.

[34] Jefferson Lab Hall B, G. Gilfoil et al., PAC32 Proposal (PR-12-07-104).

[35] A. Kotzinian, Nucl. Phys. B441 (1995) 234, hep-ph/9412283.

[36] D. Boer and P.J. Mulders, Phys. Rev. D57 (1998) 5780, hep-ph/9711485.

[37] R.N. Cahn, Phys. Lett. B78 (1978) 269.

[38] R.D. Tangerman and P.J. Mulders, Phys. Rev. D51 (1995) 3357, hep-ph/9403227.

[39] P. Reimer et al., (DY measurements: Fermilab E906).

[40] S.J. Brodsky and F. Yuan, Phys. Rev. D74 (2006) 094018, hep-ph/0610236.

[41] P.V. Pobylitsa, (2003), hep-ph/0301236.

[42] A. Bacchetta et al., JHEP 08 (2008) 023, 0803.0227.

[43] V. Barone, Z. Lu and B.Q. Ma, Phys. Lett. B632 (2006) 277, hep-ph/0512145.

[44] L.P. Gamberg, G.R. Goldstein and M. Schlegel, Phys. Rev. D77 (2008) 094016, 0708.0324.

[45] V. Barone, A. Prokudin and B.Q. Ma, Phys. Rev. D78 (2008) 045022, 0804.3024.

[46] B. Zhang et al., Phys. Rev. D78 (2008) 034035, 0807.0503.

[47] M. Anselmino et al., (2007), hep-ph/0701006.

[48] A. Bacchetta et al., Phys. Lett. B659 (2008) 234, 0707.3372.

[49] M. Anselmino et al., Phys. Rev. D71 (2005) 074006, hep-ph/0501196.

[50] HERMES, A. Airapetian et al., Phys. Lett. B562 (2003) 182, hep-ex/0212039.

[51] J.C. Collins et al., Phys. Rev. D73 (2006) 014021, hep-ph/0509076.

[52] S. Boffi et al., (2008) in preparation.

[53] B. Pasquini, S. Cazzaniga and S. Boffi, Phys. Rev. D78 (2008) 034025, 0806.2298.

[54] H. Avakian et al., JLab Experiment E12-06-015 (2008).

[55] H. Avakian et al., JLab Experiment E12-07-015 (2008).

[56] K. Hafidi et al., JLab Experiment E12-XX-XXX (2008).

[57] European Muon, J.J. Aubert et al., Phys. Lett. B130 (1983) 118.

[58] European Muon, M. Arneodo et al., Z. Phys. C34 (1987) 277.

[59] E665, M.R. Adams et al., Phys. Rev. D48 (1993) 5057.

[60] ZEUS, J. Breitweg et al., Phys. Lett. B481 (2000) 199, hep-ex/0003017.

[61] ZEUS, S. Chekanov et al., Eur. Phys. J. C51 (2007) 289, hep-ex/0608053.

[62] CLAS, . and others, (2008), 0809.1153.

[63] H. Mkrtchyan et al., Phys. Lett. B665 (2008) 20, 0709.3020.

[64] COMPASS, W. Kafer, (2008), 0808.0114.

[65] HERMES, F. Giordano, (2008), Spin-2008 proceedings.

[66] F. Garibaldi et al., Nucl. Instrum. Meth. A502 (2003) 117.

[67] M. Iodice et al., Nucl. Instrum. Meth. A553 (2005) 231.

[68] Hall-A, F. Garibaldi et al., JLab Experiment E94-107 (1994).

[69] A.S. Group, CERN Program Library Long Writeup W501 WWW://wwwinfo.cern.ch/asdoc/*geant_html*3/geantall.html (2003).

[70] CLAS, P. Rossi et al., http://www.jlab.org/∼rossi/rich/*rich_v*2.pdf (2008).

[71] J. Lachniet et al., (2008), 0811.1716.

[72] E.L. Berger, Z. Phys. C4 (1980) 289.

[73] A. Brandenburg, V.V. Khoze and D. Mueller, Phys. Lett. B347 (1995) 413, hep-ph/9410327.

[74] A. Afanasev, C.E. Carlson and C. Wahlquist, Phys. Lett. B398 (1997) 393, hep-ph/9701215.

[75] S.J. Brodsky et al., Phys. Lett. B449 (1999) 306, hep-ph/9812277.

[76] I. Akushevich, N. Shumeiko and A. Soroko, Eur. Phys. J. C10 (1999) 681, hep-ph/9903325.

[77] I. Akushevich, A. Ilyichev and M. Osipenko, (2007), 0711.4789.

[78] A. Kotzinian, Prepared for 16th International Spin Physics Symposium (SPIN 2004), Trieste, Italy, 10-16 Oct 2004.

[79] H. Avakian and P. Bosted., (2006).

[80] L. Mankiewicz, A. Schafer and M. Veltri, Comput. Phys. Commun. 71 (1992) 305.

[81] J.C. Collins, L. Frankfurt and M. Strikman, (1997), hep-ph/9709336.

[82] S.V. Goloskokov and P. Kroll, Eur. Phys. J. C53 (2008) 367, 0708.3569.

[83] M. Strikman and C. Weiss, (2008), 0804.0456.

[84] M. Diehl et al., Phys. Rev. D72 (2005) 034034, hep-ph/0506171.

[85] Jefferson Lab Hall B, . H.Avakian et al., LOI to PAC34 (2008).

[86] B. Zhang et al., Phys. Rev. D77 (2008) 054011, 0803.1692.

[87] FNAL E866/NuSea, L.Y. Zhu et al., Phys. Rev. Lett. 100 (2008) 062301, 0710.2344.

[88] A. Metz and M. Schlegel, Eur. Phys. J. A22 (2004) 489, hep-ph/0403182.

[89] X. Ji et al., Phys. Rev. D73 (2006) 094017, hep-ph/0604023.

[90] A. Schafer and O.V. Teryaev, Phys. Rev. D61 (2000) 077903, hep-ph/9908412.